The ternary complex CEP90, FOPNL and OFD1 specifies the future location of centriolar distal appendages, and promotes their assembly

Pierrick Le Borgne[1], Marine Hélène Laporte[2], Logan Greibill[1], Michel Lemullois[1], Mebarek Temagoult[3], Olivier Rosnet[4], Maeva Le Guennec[2], Laurent Lignières[5], Guillaume Chevreux[5], France Koll[1], Virginie Hamel[2], Paul Guichard[2], Anne-Marie Tassin[1]

1- Université Paris-Saclay, CEA, CNRS, Institute for Integrative Biology of the Cell (I2BC), 91198, Gif-sur-Yvette, France
2- University of Geneva, Department of Cell Biology, Geneva, Switzerland
3- Imagerie-Gif Light facility, Université Paris-Saclay, CEA, CNRS, Institute for Integrative Biology of the Cell (I2BC), 91198, Gif-sur-Yvette, France
4- Centre de Recherche en Cancérologie de Marseille (CRCM), Aix Marseille Univ, CNRS, INSERM, Institut Paoli-Calmettes, 13009 Marseille, France.
5- ProteoSeine@IJM, Université de Paris/CNRS, Institut Jacques Monod, 75006 Paris, France

Abstract

Cilia assembly starts with centriole to basal body maturation, migration to the cell surface and docking to the plasma membrane. The basal body docking process involves the interaction of both the distal end of the basal body and the transition fibers (or mature distal appendages), with the plasma membrane. During this process, the transition zone assembles and forms the structural junction between the basal body and the nascent cilium. Mutations in numerous genes involved in basal body docking and transition zone assembly are associated with the most severe ciliopathies, highlighting the importance of these events in cilium biogenesis.

The conservation of this sequence of events across phyla is paralleled by a high conservation of the proteins involved. We identified CEP90 by BioID using FOPNL as a bait. Ultrastructure expansion microscopy showed that CEP90, FOPNL and OFD1 localized at the distal end of both centrioles/basal bodies in *Paramecium* and mammalian cells. These proteins are recruited early after duplication on the procentriole. Finally, functional analysis performed both in *Paramecium* and mammalian cells demonstrate the requirement of this complex for distal appendage assembly and basal body docking. Altogether, we propose that this ternary complex is required to determine the future position of distal appendages.

Introduction

The centrosome is the main microtubule organizing center in most animal cells. It is composed of two centrioles, microtubules based organelles displaying a nine-fold symmetry, surrounded by layers of pericentriolar material (Paintrand *et al*, 1992), (Tassin & Bornens, 1999), (Mennella *et al*, 2014). A structural asymmetry between the two centrioles is observed, the mother one, bearing distal and subdistal appendages, while the daughter lacks these appendages (Paintrand *et al*, 1992). In resting cells, the mother centriole matures into a basal body (BB), which functions as a platform to template the assembly of a cilium. Cilia can be found at the cell surface either unique or in multiple copies, motile or unmotile (Mitchison & Valente, 2017). They are highly conserved organelles from protist to mammalian cells in terms of structure and protein composition (Vincensini *et al*, 2011). In all cases, cilia possess mechano- and chemo-sensitivity properties. In addition, motile cilia beat to generate a flow such as cerebral fluid (brain ventricle), mucus (respiratory tract) or the forces required to propulse the cells (spermatozoid, ovum, unicellular organisms) (Mitchison & Valente, 2017).

Ciliogenesis is a multistep process involving: BB duplication, migration to the cell surface and anchoring of the mother centriole, followed by ciliary growth. These steps are common to all systems, although variations in some steps may exist between different organisms or between cellular types within a given organism, (Sorokin, 1962), (Garcia-Gonzalo & Reiter, 2017), (Wiegering *et al*, 2018), (Vieillard *et al*, 2016). The conservation of this sequence of events across phyla is paralleled by a high conservation of the proteins involved (Vincensini *et al*, 2011), (Jana *et al*, 2014).

The BB anchoring process, which occurs both during ciliogenesis and formation of the immunological synapse, requires the tethering between the distal appendages, which in mammalian cells contain Cep83, Cep89, SCLT1, FBF1 and Cep164 (Tanos *et al*, 2013), (Joo *et al*, 2013), (Failler *et al*, 2014), (Yang *et al*, 2018) and a membrane. This membrane could be either Golgi-apparatus derived-vesicles membrane that fuse together to form the ciliary shaft, as in most metazoan cells, or the plasma membrane

directly as in some mammalian cell types such as the immunological synapse (Stinchcombe *et al*, 2015) or in *Paramecium*. The interaction of the BB with the membrane leads to the formation of the transition zone (TZ), bridging the BB to the axoneme, which has recently been recognized to act as a diffusion barrier between the intracellular space and the cilium, defining the ciliary compartment (Reiter *et al*, 2012), (Gonçalves & Pelletier, 2017). Mutations in genes encoding proteins localized at the BB distal end, distal appendages and TZ lead to various syndromes in humans, called ciliopathies, (Oro-facial-digital, Nephronophtysis, Joubert), reinforcing the importance to study and understand how these structures and the proteins that compose it are controlling ciliogenesis (Singla *et al*, 2010), (Lopes *et al*, 2011a), (Thauvin-Robinet *et al*, 2014), (Failler *et al*, 2014), (Chevrier *et al*, 2016).

The ternary complex composed of OFD1 (Lopes *et al*, 2011), FOPNL/FOR20 (Sedjaï *et al*, 2010) and OFIP/MNR/KIAA0753 (Kodani *et al*, 2015), (Kumar *et al*, 2021) has been localized in mammalian cells at the centriole distal end and at the centriolar satellites, membrane-less cytoplasmic granules that concentrate in the vicinity of the centrosome (Kubo & Tsukita, 2003). OFIP was shown to interact directly with FOPNL and OFD1 (Chevrier *et al*, 2016), two proteins required for building the distal end of the basal bodies and for the anchoring process in both mammalian cells (Singla *et al*, 2010), (Thauvin-Robinet *et al*, 2013) and *Paramecium* (Aubusson-Fleury *et al*, 2012), (Bengueddach *et al*, 2017). In mammalian cells, the dual location of these proteins at both distal end and centriolar satellites (Sedjaï *et al*, 2010),(Singla *et al*, 2010) (Chevrier *et al*, 2016) prevents from determining, which pool is involved in BB anchoring process, since centriolar satellites are also involved in cilia formation (Sedjaï *et al*, 2010), (Stowe *et al*, 2012). Interestingly, a recent study using satellites-less PCM1-/- cells demonstrated that the centriolar pool of the complex composed of MNR, OFD1 and CEP90 is crucial for ciliogenesis (Kumar et al. 2021). In this paper, we turn to *Paramecium* as a physiological model, devoid of centriolar satellites, as far as we can tell from electron microscopy studies and by the absence of PCM1 orthologues, to further demonstrate the requirement and the evolutionary conservation of the BB distal end proteins FOPNL/FOR20 together with OFD1 and CEP90 in the BB anchoring process (Aubusson-Fleury *et al*, 2012), (Bengueddach *et al*, 2017).

However, the function in ciliogenesis of OFIP/MNR/KIAA0753 in *Paramecium* is not conserved (Koll, personal communication), despite the presence of a small conserved domain (Chevrier *et al*, 2016).

Paramecium tetraurelia is a free-living unicellular organism, easy to cultivate that bear at its surface ca. 4000 cilia. The corresponding BB are arranged in longitudinal rows, and their polarity is marked by the asymmetrical organization of their associated appendages (Iftode *et al*, 1989), (Tassin *et al*, 2015). In *Paramecium*, BB organization is highly precise, with regions composed of units with singlet or doublet BB. Units with doublets BB can display either 2 ciliated BB or a ciliated and an unciliated one (Iftode *et al*, 1989). Interestingly, the TZ matures biochemically and structurally between the two states (Gogendeau *et al*, 2020). Unlike metazoa, there is no centriolar stage in *Paramecium:* new BB develop from the docked ones. Once duplicated, they just have to tilt-up for anchoring directly at the surface. Due to the high number of BB at the cell surface, defective BB anchoring process is easily detected in *Paramecium* by immunofluorescence (IF), making of *Paramecium* an outstanding model to characterize new partners in the BB anchoring process. As a proof of concept, we demonstrated the functional conservation of both FOPNL (Aubusson-Fleury *et al*, 2012) and OFD1 (Bengueddach *et al*, 2017) in BB anchoring process in *Paramecium.*

In order to identify new proteins involved in BB docking, we reasoned that proteins located at proximity of a known BB anchoring protein could be acting in the same process. Therefore, we identified proteins at proximity of FOPNL/FOR20 proteins by BioID in human cells followed by mass spectrometry. Among the candidate proteins, we focused our study on, CEP90/PIBF1, whose mutations in the *CEP90* gene lead to both Jeune and Joubert (Wheway *et al*, 2015), (Shen *et al*, 2020) syndromes suggesting defective ciliogenesis. In addition, CEP90 is conserved from protist to Human, despite being absent in some groups as drosophilidae or rabditidae. Functional analysis performed both in *Paramecium* and mammalian cells using RNAi demonstrates the involvement of CEP90 in the BB anchoring process. We show that CEP90 is required to build the distal end of the BB, as previously shown in *Paramecium* for OFD1 and FOPNL/FOR20. Using ultrastructure expansion microscopy (U-ExM), we demonstrate that CEP90 and

OFD1 proteins localize, in both Paramecium and U2OS cells, at the distal end of BB in a 9-fold symmetry. Both CEP90 and OFD1 associate early with nascent procentrioles in human cells and stay associated with their distal tips during centrioles elongation, as already known for FOPNL and OFD1 in *Paramecium* (Aubusson-Fleury *et al*, 2012), (Bengueddach *et al*, 2017). We demonstrate that CEP90 is recruited at the centriolar distal end together with OFD1 and FOPNL both in *Paramecium* and mammalian cells. The early recruitment of both CEP90 and OFD1 on procentrioles, led us to propose that these proteins specify the future distal appendage location. We show that CEP90 together with FOPNL and OFD1 are necessary to recruit distal appendages proteins in mammalian cells. In conclusion, our results demonstrate that these proteins build the centriole/BB distal ends and allow BB docking at cell membrane.

Results

To discover novel proteins involved in the BB anchoring process, BioID was performed using FOPNL as a bait in human cells. To do so, Flp-In HEK293 cells expressing myc-BirA*-FOPNL under the control of the tetracycline repressor were generated. Centrosomal biotinylated proteins were purified on streptavidin beads and analyzed by mass spectrometry. Candidates were ranked according to their fold change and p-value. According to these criteria, several known BB anchoring proteins such as Talpid3 (Kobayashi *et al*, 2014), OFIP/MNR/KIAA0753 (Chevrier *et al*, 2016), PCM1 (Sedjaï *et al*, 2010) were enriched in our mass spectrometry validating our approach (see Table S1). In addition, some novel potential interactors were found. We focused further our functional analysis on the candidate centriolar protein CEP90/PIBF1 as: i) *Cep90* gene was found mutated in ciliopathies (Wheway *et al*, 2015).; ii) *Cep90* is well conserved from unicellular to mammalian cells.

Paramecium CEP90-GFP localizes to basal body

As *Paramecium* appears as an outstanding model to decipher the BB anchoring process, we searched for CEP90 homologs in *Paramecium tetraurelia*. Two CEP90 homologs, CEP90a and CEP90b, derived from the last whole genome duplication (Aury *et al*, 2006) were identified. RNAseq analysis of the *P. tetraurelia* transcriptome during vegetative growth revealed that CEP90a is 24x more expressed than CEP90b (Arnaiz *et al*, 2010, and paramecium.i2bc.paris-saclay.fr).

To ascertain the localization of CEP90 in *Paramecium*, we expressed CEP90a-GFP-tagged, since it is the most expressed protein, under the control of the constitutive calmodulin gene-regulatory elements. After transformation, rows of GFP dots were observed on transformants displaying a wild type growth rate and phenotype (Figure 1A). Labelling with an antibody directed against tubulin poly-glutamylation (poly-E), which decorates BB (Gogendeau et al, 2020), showed that this GFP signal corresponded to the BB (Figure 1A). This staining is reminiscent of the GFP-FOPNL (Figure 1B) and OFD1-GFP staining (Aubusson-Fleury *et al*, 2012), (Bengueddach *et al*, 2017), as expected for a proximity partner. A careful

observation of the GFP staining pattern relative to the BB, revealed that all BB are decorated, i.e., ciliated and unciliated, (Figure 1A, magnification), unlike the GFP-tagged MKS and NPHP protein complex, which stained only ciliated BB (Gogendeau *et al*, 2020). Double labelling of CEP90-GFP cells using poly-E antibodies and anti-epiplasm (Jeanmaire-Wolf *et al*, 1993), a superficial cytoskeleton layer, which embeds the BB, revealed that the CEP90-GFP staining is restricted at BB distal ends (Figure 1A', magnification) similar to GFP-FOPNL staining (Figure 1B', magnification).

The ternary complex CEP90, FOPNL and OFD1 localizes at the basal body distal ends in a 9-fold symmetry in Paramecium

To characterize more precisely the localization of CEP90 together with FOPNL and OFD1, we used U-ExM (Gambarotto *et al*, 2019), (Gambarotto *et al*, 2021). Since *Paramecium* is 150 µm long and 50µm thick, U-ExM was performed on isolated cortexes (Le Guennec *et al*, 2020) from *Paramecium* expressing GFP-FOPNL, CEP90-GFP or OFD1-GFP to allow a nanoscale localization of these proteins within the structure (Figure 1C-G). During cortex purification, we observed ciliary shedding just above the TZ (Figure S1A), as it is known to occur in physiological conditions (Adoutte *et al*, 1980), (Gogendeau *et al*, 2020). Double stained longitudinally oriented BB show that in CEP90-GFP paramecia, the GFP staining was located either at the top of the BB assessed by the anti-tubulin staining (Figure S1B, yellow arrowhead) or slighlty underneath (Figure 1C, S1B). This observed difference could be associated with the ciliation status, since ciliated BB showed a longer TZ with extended microtubule doublets than unciliated ones (Figure S1A); (Tassin *et al*, 2015), (Gogendeau *et al*, 2020). Therefore, we propose that the staining is found at the proximal part of the TZ on all BB and the observed tubulin staining above the GFP staining might be associated to ciliated BB (Figure 1C-E, Figure S1) and would correspond to the elongation of the TZ that occurs during ciliogenesis. Longitudinally oriented BB stained for OFD1-GFP (Figure 1D, Figure S1C) and GFP-FOPNL (Figure 1E, Figure S1D-E) BB show a similar pattern than CEP90-GFP, suggesting that these three proteins localized at the end of the BB or at the proximal part of the TZ (Figure 1C-E, F). Moreover, analysis of the protein's positions along the microtubule wall indicated that all three proteins

localize at the same average position at around 425 nm from the proximal extremity (Figure 1F). Observations on top-viewed BB showed that the three proteins were organized in a 9-fold symmetry, close to the microtubule wall but externally (Figure 1C', D', E'). Quantification of the distance between both GFP and tubulin maximal intensity signal of the rings revealed that CEP90-GFP, OFD1-GFP and GFP-FOPNL localized close to the microtubule wall with CEP90 and FOPNL appearing at around 15 nm away from the microtubule wall, while OFD1 was at around 30 nm, suggesting that OFD1 is more external than the 2 others (Figure 1G). This localization was further refined by immunogold staining of CEP90-GFP on whole permeabilized cells in which the gold particles were found mostly at the level of the TZ, close to the microtubular wall (Figure 1I-K). Counting of gold particles confirmed that most of the particles are localized at the proximal part of the TZ (65%) (Figure 1J).

CEP90 depletion prevents basal body docking in Paramecium

Since CEP90 was found at proximity of FOPNL by BioID and localized similarly as OFD1-GFP and GFP-FOPNL, we predicted that it will be involved in BB anchoring through its contribution in building the BB distal end. To test this hypothesis, we first decided to knock-down *CEP90* in *Paramecium* by feeding wild-type cells with dsRNA-producing bacteria to induce RNA interference (Galvani & Sperling, 2002). As a control, we inactivated the unrelated gene *ND7*, involved in the exocytosis of trichocystes, using the same protocol. The high percentage of identity between *CEP90a* and *CEP90b* genes made difficult to design RNAi constructs to inactivate each gene individually. Therefore, we silenced them both together. The efficiency of the vector to inactivate its target was tested by verifying the effective depletion of GFP-CEP90a by immunofluorescence (Figure 2B, Figure S2A). *CEP90* knock-down induced a slowdown of cellular growth and cellular death after 3/4 divisions (Figure S2B). A modification of the cell size and cell shape was observed from the first division. *Paramecia* appeared smaller and rounder after *CEP90* inactivation (Figure 2A,CEP90^{RNAi}). The swimming velocity was also reduced, as previously observed for defective BB (Figure S2C, Gogendeau et al, 2020). To analyze the effects of the depletion on the BB, inactivated cells were labeled for BB using poly-E antibodies. Whereas, control depleted cells (Ctrl RNAi)

display BB at the cell surface organized in longitudinal rows (Figure 2A, cortex), Cep90-depleted cells show misaligned BB at the cortical surface (Figure 2A, CEP90^{RNAi}). Confocal microscopy demonstrated that numerous BB were found in the cytoplasm after CEP90 depletion, suggesting BB anchoring defects (Figure 2A', CEP90^{RNAi}), while none were observed in control depleted cells (Figure 2A', Ctrl^{RNAi}). To ascertain the specificity of this phenotype, RNAi resistant CEP90a-GFP transformants were inactivated by CEP90a/b RNAi. GFP staining of RNAi resistant CEP90-GFP transformants decorated BB as revealed by poly-E antibodies as CEP90-GFP (Figure 2C cortex, magnification). In addition, cytoplasmic aggregates were observed most probably due to the protein overexpression (Figure 2C cytoplasm and magnification). Cells were then analyzed for swimming velocity, cell viability and BB organization. RNAi resistant GFP-CEP90a paramecia inactivated for CEP90 divide about 4 times a day, as controldepleted cells, and do not die anymore (Figure S2B). Similarly, the swimming velocity of RNAi resistant CEP90a-GFP paramecia was also restored (Figure S2C). Finally, the expression of RNAi resistant CEP90a-GFP on CEP90-depleted cells rescue BB organization at the cell surface (Figure 2C). Those cells display longitudinal rows of BB (Figure 2C), while CEP90a-GFP transformants inactivated for CEP90 display numerous BB in the cytoplasm (Figure 2B). The misaligned BB at the cell surface and cytoplasmic BB observed after CEP90 depletion is reminiscent of the phenotypes observed after depletion ofeither of FOPNL or OFD1 depletion (Figure 2 A, A', FOPNL^{RNAi}) and (Aubusson-Fleury *et al*, 2012) (Bengueddach *et al*, 2017)). Altogether, these results suggest that CEP90 is involved in BB anchoring process in *Paramecium*.

To understand this BB anchoring defect, we analyzed by electron microscopy the ultra-structure of the undocked BB. Control depleted cells show BB anchored at the cell surface and displaying the characteristic three plates of the BB TZ (arrowheads on Figure 3A). In contrast, in CEP90 depleted cells, numerous BB were lying in the cytoplasm. All of them, display defective distal ends with vestigial structures resembling the intermediate (blue arrowhead) and axosomal (magenta arrowhead) plate, while the terminal plate (green arrowhead) was mostly absent (Figure 3B-E). Occasionally, microtubule extensions were observed on the uncapped side of the BB (Figure 3E, white arrow).

In mammalian cells, CEP90 seems required for centrosome duplication (Kodani *et al*, 2015). Therefore, we decided to determine if it was also required for BB duplication in *Paramecium*. CEP90 depleted cells undergoing their second division under silencing conditions were stained for BB. The depletion of CEP90 did not disturb BB duplication, as demonstrated by the characteristic longitudinal groups of three or four BB issued from parental groups of two (Figure S3). This result suggests that in *Paramecium* CEP90 is not involved in the BB duplication process.

Taken together, these results indicate that CEP90 in *Paramecium* is required to build the distal ends of BB, which is necessary to dock the BB at the cell surface, as already observed for both FOPNL and OFD1.

CEP90, FOPNL and OFD1 are required for basal body distal end assembly in Paramecium

In *Paramecium*, like FOPNL (Aubusson-Fleury *et al*, 2012), and OFD1 (Bengueddach *et al*, 2017), Centrin2 (Ruiz *et al*, 2005), have been shown to be required to assemble the BB distal end. Centrin2 is recruited first and initiates the assembly of the three plates found at the BB distal end of the TZ. This step is followed by a co-recruitment of both FOPNL and OFD1 (Aubusson-Fleury *et al*, 2012) (Bengueddach *et al*, 2017). Finally, Centrin3 is recruited to allow the tilting-up of the BB after duplication in order to let the BB to anchor (Jerka-Dziadosz *et al*, 2013). BB of Centrin3-depleted cells are nicely assembled, and display the three plates of the TZ, characteristic of unciliated docked BB.

To determine the involvement of CEP90 in distal end assembly, paramecia expressing GFP-tagged proteins (Centrin2, CEP90, OFD1, FOPNL) were inactivated by either Centrin2, OFD1, FOPNL, CEP90 and Centrin3 RNAi as well as control RNAi. The fate of fluorescence in each transformed cells was followed after two/three divisions under RNAi conditions by immunostaining (Figure 4A) and the remaining fluorescence was quantified in each case (Figure 4B-D). The recruitment of CEP90-GFP to BB, required the presence of FOPNL and OFD1 (Figure 4A, 4B). Reciprocally, CEP90 depletion prevented the recruitment of GFP-FOPNL (Figure S4A, S4B) and OFD1-GFP (Figure 4A, 4D). As expected from this

result, cells depleted for FOPNL, OFD1, or CEP90 maintained the recruitment of Centrin2 on newly formed BB (Figure 4A, C). We demonstrated that Centrin2 depletion prevented the recruitment of CEP90 and OFD1 to the newly formed BB (Figure S4C, Figure 4B, 4D). By contrast, the depletion of Centrin3, which is not involved in the distal end assembly, did not affect the recruitment of Centrin2-GFP, CEP90-GFP and OFD1-GFP (Figure S4D, Figure 4 B-D). Therefore, we propose that CEP90-GFP, GFP-FOPNL and OFD1-GFP are co-recruited at the BB to assemble its distal end.

Altogether, these results obtained in *Paramecium* show that CEP90, FOPNL and OFD1 localize similarly as suggested by the U-ExM. The interdependent recruitment of this ternary complex is involved in BB distal end maturation, allowing the BB anchoring process.

Mammalian CEP90 and OFD1 localize at the distal end of mother and daughter centrioles as well as procentrioles

To investigate the functional conservation of CEP90 throughout the evolution, we analyze CEP90 function in mammalian cells. In RPE1 cells, CEP90 localizes, at centrioles and centriolar satellites, as previously shown by Kodani *et al*, (2015) reminiscent of FOPNL (Sedjaï *et al*, 2010) and OFD1 (Lopes *et al*, 2011) (Figure 5A, B and Figure S5A). To assess the function of CEP90 during mammalian ciliogenesis, we first use U-ExM to resolve its localization at nanoscale resolution. We observed first that, in dividing cells, the endogenous CEP90 or OFD1 longitudinal fluorescence signal is restricted to the centriolar distal end as compared to the tubulin signal, which depicts the whole centriolar length (Figure 5C, D, F and G). The precise measurement of both CEP90 and OFD1 staining revealed that these two proteins localize on the two parental centrioles at about 375 nm from their proximal centriolar extremity (Figure 5I), about 50nm from their distal end of the centrioles. From top-viewed centrioles, we observed a staining organized in a 9-fold symmetry close to the external surface of the centriolar microtubule wall (Figure 5 E, H, J). The measurements of both CEP90 and OFD1 stainings relative to the tubulin maximal intensity signal show that CEP90 is slightly closer to the microtubule wall than OFD1 (average distance between CEP90 and

tubulin about 30 nm, while OFD1 is about 40 nm) (Figure 5 K). Unfortunately, we have not been able to localize FOPNL using U-ExM, since our antibodies were not working under these conditions. Importantly, the analysis of both CEP90 and OFD1 staining during centriole duplication showed that both proteins were recruited on procentrioles (Figure 5C, D, F, G). Altogether, these results obtained by U-ExM demonstrate that the nanometric localization of both CEP90 and OFD1 in mammalian cells is similar to the one observed in *Paramecium*, the slight differences being most probably due to the fact that in *Paramecium* cells, BB are anchored at the cell membrane, whereas in mammalian cells, our observations arise from non-ciliated centrioles. The conserved localization between two evolutionary distant organisms might suggest a conserved function.

The co-recruitment of CEP90, FOPNL, OFD1 is required for the formation of distal appendages

Next, we investigated the hierarchy of recruitment of these three proteins to the centriole distal end in RPE1 cells. We first inactivated either *CEP90* or *FOPNL* gene using 2 sets of siRNA for each gene and found a significant reduction in CEP90 (about 80%) and FOPNL (about 90%) levels respectively at the centrosome (Figure 6A-C) demonstrating the efficiency of the siRNA, as previously reported (Kodani *et al*, 2015), (Sedjaï *et al*, 2010). Next, we analyzed the recruitment of CEP90, FOPNL and OFD1 to the centrioles upon depletion of CEP90 or FOPNL. We demonstrated that the recruitment of endogenous FOPNL and OFD1 at the centrosome was decreased of about 66% upon CEP90 depletion (Figure 6A, B, D). Similarly, the depletion of FOPNL decrease the localization of both CEP90 and OFD1 to the centrioles of about 66% (Figure 6A, C, D). These results suggest that the inter-dependant recruitment of CEP90, FOPNL, OFD1 to centrioles and BB is conserved in *Paramecium* and mammalian cells.

To gain further insights into the role of CEP90, OFD1 and FOPNL in ciliogenesis, we depleted either CEP90 or FOPNL protein in serum-starved RPE1 cells. As expected from previous results (Kim *et al*, 2012), (Sedjaï *et al*, 2010), (Chevrier *et al*, 2016), we observed a significant decrease in cilia formation (about 66% compared to control siRNA) (Figure S5B) for both CEP90 and FOPNL siRNA treated cells.

Since we demonstrated in *Paramecium* that the ternary complex is involved in BB docking by affecting the BB distal end, we investigated the formation of distal appendages after depletion of one member of the complex. Distal appendage formation requires both removal of daughter specific proteins (Wang *et al*, 2018) and specific proteins able to recruit them. First, we analyzed if the depletion of CEP90 and FOPNL may affect the behavior of one daughter centriolar protein (DCP), Centrobin. As shown on Figure S6, we did not observe any difference in the localization of Centrobin in control and CEP90 or FOPNL depleted cells. Secondly, we investigated the localization of the most proximal distal appendage protein CEP83, together with CEP89 and CEP164. We showed that the depletion of either CEP90 or FOPNL decreased the localization at the mother centriole of these three proteins of about 66% (Figure 6A, B). Altogether, these results suggest that the depletion of CEP90 and FOPNL prevents the formation of the distal appendages as previously shown for OFD1. Consequently, BB docking at a ciliary vesicle cannot occur, leading to defective ciliogenesis.

Discussion

The search of proximity partners of FOPNL in mammalian cells led us to identify CEP90. As expected from previous results, we identified in our mass spectrometry MNR/OFIP in proximity of FOPNL (Chevrier *et al*, 2016), (Kumar *et al*, 2021). Interestingly, these two proteins are working in a complex with OFD1 to build a cilium (Lopes *et al*, 2011a). Surprisingly, OFD1 is not significantly found despite the presence of biotinylated peptides. In addition, several centriolar satellite proteins as PCM1, CEP350, Cep131 or Talpid3 were significantly detected in proximity to FOPNL in our mass spectrometry, consistent with previous work (Gheiratmand *et al*, 2019). In agreement with our mass spectrometry results, CEP90 was previously identified as a centrosomal and centriolar satellite protein. Previously, CEP90 has been involved in spindle pole integrity in mitotic cells (Kim *et al*, 2012) or in centrosome duplication, by recruiting CEP63 to the centrosome (Kodani *et al*, 2015). The analysis in *Paramecium* of the effect of CEP90 depletion on BB duplication shows no duplication defects. Two hypotheses may explain this result. First, *Paramecium* cells being devoid of centriolar satellites, our results could suggest that it is most probably the centriolar satellite pool that is involved in BB duplication to target CEP63 to the centrosome, reinforcing previous results (Kodani *et al*, 2015). Another possible explanation would be that, despite numerous actors being conserved (Jerka-Dziadosz *et al*, 2010), (Gogendeau *et al*, 2011) (Klotz *et al*, 2003), (Ruiz *et al*, 2000), (Dupuis-Williams *et al*, 2002), some proteins are not, such as CEP63, suggesting that the mechanism of BB duplication might differ between *Paramecium* and mammalian cells.

The ternary complex CEP90, FOPNL and OFD1 is required for basal body anchoring

Patients showing *CEP90* mutations and displaying Joubert and Jeune syndromes, two ciliopathies, led Kim et al (2012) to postulate that CEP90 function in ciliogenesis may occur through centriolar satellites since their disruption inhibits the ciliogenesis process. To determine if CEP90 functions at centrioles or at satellites during ciliogenesis, we took advantage of the *Paramecium* model, which does not possess centriolar satellites, simplifying the read out of the underlying phenotype. We found that CEP90 depletion

in *Paramecium* prevents BB distal end formation as previously shown for FOPNL and OFD1, resulting in unanchored BB that remain in the cytoplasm. Interestingly, the depletion of CEP90 prevents maturation of the distal end of BB at the same step as FOPNL or OFD1 (Aubusson-Fleury *et al*, 2012), (Bengueddach *et al*, 2017) as observed by electron microscopy. This suggests that CEP90, FOPNL and OFD1 are working together to constitute a functional ternary complex. Two other arguments suggest that it is the case. First, expansion microscopy performed both in *Paramecium* and mammalian cells, demonstrate that the three proteins localize similarly, close and external to the microtubule wall in a 9-fold symmetry. Secondly, the depletion of one of these proteins in *Paramecium* prevents the recruitment of the two others. Similar results were obtained in mammalian cells.

In mammalian cells, the initial step of BB anchoring requires an interaction between the distal appendages and a cellular membrane (Knödler *et al*, 2010), (Westlake *et al*, 2011), (Schmidt *et al*, 2012), (Sillibourne *et al*, 2013), (Tanos *et al*, 2013), (Shakya & Westlake, 2021). Remarkably, we found that either CEP90 or FOPNL depletion prevents the recruitment of the most proximal distal appendage protein CEP83 as well as CEP89 and CEP164, suggesting that the assembly of distal appendages is strongly impaired in these depleted cells. This result is reminiscent of OFD1 depletion, which prevents the assembly of distal appendages (Singla *et al*, 2010). Altogether, these results indicate that the ternary complex composed of CEP90, FOPNL and OFD1 is required to tether the BB at a membrane in *Paramecium* and mammalian cells. Interestingly, *Paramecium* and mammalian cells use two distinct BB anchoring pathways. In *Paramecium*, the BB anchors directly to the cell membrane, whereas in RPE1 mammalian cells, cytoplasmic vesicles are recruited to the distal appendages, fuse to form the ciliary vesicle, in which the axoneme elongates, suggesting a functional conservation of this molecular complex in these two evolutionary distant organism. Intriguingly, these proteins are absent in the *drosophila* and *C. elegans* genome. A possible explanation might be that in these species, the mechanism of BB anchoring might differ due to the absence of centriolar distal appendage structures. Interestingly, Hou et al (in revision)

demonstrate in *Drosophila*, that the distal appendage proteins CEP89, FBF1 and CEP164 are not required for BB docking and TZ formation, despite their recruitment, in a 9 fold symmetry, during BB anchoring.

The ternary complex points out the future position of distal appendages assembly

The examination of the localization of either CEP90, FOPNL or OFD1 by U-ExM in *Paramecium* and mammalian cells established that these proteins localize at the distal end in a 9-fold symmetry. U-ExM quantification in addition to EM results suggest that CEP90 staining remains at the same position along the MT while TZ maturation occurs. As previously described, a structural lengthening of the TZ (Gogendeau *et al*, 2020) occurs during ciliary growth. CEP90 localizes to all BB whatever their ciliation status at the most proximal part of the TZ as observed by immunogold staining in EM. This is in contrast with the TZ proteins belonging to either MKS or NPHP complex or the regulators of TZ assembly CEP290 and RPGRIP1L, which are recruited only on at the distal part of the TZ of ciliated BB. In *Paramecium*, the transition fibers emerge from the microtubule doublets at the level of the intermediate plate (Dute & Kung, 1978), a position compatible with our U-ExM and immunogold staining.

In agreement with the *Paramecium* staining, in mammalian cells both the mother and the daughter centrioles are decorated. However, the staining is observed slightly underneath the extreme end of the centriole. This localization is compatible with the localization of CEP83 along the BB proximo-distal axis (Bowler *et al*, 2019). Examination of centrioles during the duplication process, demonstrates that either CEP90 or OFD1 are recruited on the newly born procentriole at a subdistal position similar to the one observed on mature centriole. This result differs from the one (Kumar *et al*, 2021), which reports the recruitment of the MNR, CEP90, OFD1 complex on elongating procentrioles in G2. This discrepancy might be due to the fact that these authors used 5-ethynyl-29-deoxyuridine (EdU) to distinguish the different phases of the cell cycle, while we used unsynchronized U2OS cells. Another possibility is that the recruitment of the complex differs between cell types causing this difference between our study (Kumar *et al*, 2021) which used RPE1 cells. Consistent with our findings, numerous distal end proteins such as

C2CD3, CP110, Centrin2 (Thauvin-Robinet *et al*, 2014), (Kleylein-Sohn *et al*, 2007), (Paoletti *et al*, 1996) have already been observed on newly born procentrioles. However, the precise localization of these distal end proteins show differences, C2CD3 beeing localized internally of the centriolar microtubule wall, while CP110 is at the extreme distal end. Therefore, the localization of the complex slightly underneath the distal end together with the early recruitment on procentriole led us to propose that the presence of the complex on the microtubule wall will mark the future position on which the distal appendages will assemble. However, the reason for the localization of these proteins at the distal ends on both mother and daughter centriole is not yet clear. A possible explanation might come from the results of Wang et al, (2018), showing that daughter centriolar proteins (DCP) are observed on both mother and daughter centrioles after depletion of either C2CD3 and Talpid3, which prevents distal appendages assembly, suggesting that DCP are removed from the mother centriole before distal appendages assembly. By contrast, the removal of OFD1 maintained the asymmetric localization of Centrobin on the daughter centrioles (Wang *et al*, 2018). In agreement, the depletion of either CEP90 or FOPNL maintains the asymmetry of the two centrioles by maintaining Centrobin only on the daughter centriole. Therefore, we propose the following model: the ternary complex composed of CEP90, FOPNL and OFD1 is recruited soon after centrosome duplication on the two procentrioles, slightly underneath the extreme distal end. POC1B (Chang *et al*, 2016) and POC5 (Azimzadeh *et al*, 2009) are then recruited to allow centriole elongation. Centrin2 (Ruiz *et al*, 2005), (Aubusson-Fleury *et al*, 2012), OFD1 (Singla *et al*, 2010) and MNR (Kumar *et al*, 2021) have been shown to participate in the regulation of microtubule wall length, since their absence lead to elongated centrioles. Maturation of the daughter centriole in mother is carried out by first removing daughter centriole proteins and secondly by the recruitment of distal appendage proteins (Wang *et al*, 2018), (Bowler *et al*, 2019), (Viol *et al*, 2020) during G2/M (Figure 7). A similar scenario might also been conserved in *Paramecium* since the daughter centriole protein CEP120 is conserved. It will be interesting to determine in this model the fate of CEP120 during the BB anchoring process.

Material and methods

P. tetraurelia strains and cultures conditions

The wild type reference strain, stock d4-2 of *Paramecium tetraurelia*, was used in RNAi experiment. To facilitate the screening of transformants in microinjection experiments, the mutant *nd7-1* (Skouri & Cohen, 1997) which carries a mutation preventing trichocyst exocytosis was used. Cells were grown at 27°C in wheatgrass infusion (BHB) bacterized with Klebsiella pneumoniae and supplemented with 0.8 µg/mL of β-sitosterol according to standard procedures(Sonneborn, 1970).

Human cell lines and culture condition

The human retinal pigment epithelium (RPE1), human embryonic kidney (HEK293), human bone osteosarcoma (U2OS) cell lines were grown in DMEM/F12 (RPE1), DMEM (HEK293, U2OS), respectively supplemented with 10% of Fetal bovine serum and Penicillin-streptomycin (1000 units/mL and 1000µg/mL respectively HyClone), Glutamax cultured in the presence of 5% CO2. Flp-In T-REx HEK293 cells were grown in DMEM supplemented with 10% FBS, GlutaMAX, zeocin (100 µg/mL), and blasticidin (3µg/mL). Flp-In T-REx HEK293 stable lines expressing myc-BirA* or myc-BirA*-FOPNL were maintained as above, with the addition of hygromycin (200 µg/mL) instead of zeocin.

Antibodies

The following antibodies were used: the polyclonal PolyE (1:100) antibody(Janke & Bulinski, 2011) stained cilia. For mammalian cells, polyclonal rabbit anti-CEP90 (1/500- Proteintech 14413-1-AP ((Kodani *et al*, 2015)), anti-OFD1 (1/500, Sigma HPA031103 (Wang *et al*, 2013)), anti-CEP83 (1/500- Proteintech 26013-1AP, (Hossain *et al*, 2020)), anti-Cep89 (1/800- Proteintech 24002-1AP, (Kanie *et al*, 2017)), Cep164 (1/1000- Proteintech 22227-1AP, (Bowler *et al*, 2019)), anti-Centrobin (1/500-mouse-Abcam-Ab70448 (Wang *et al*, 2018)) and monoclonal anti-FOPNL antibodies (1/200- (Sedjaï *et al*, 2010)) were used. Monobodies AA344 (1:250, scFv-S11B, Beta-tubulin) and AA345 (1:250, scFv-F2C, Alpha-tubulin;

(Nizak *et al*, 2003) were used in expansion microscopy to stain for the microtubule wall. Goat anti-rabbit Alexa Fluor 488 F(ab')2 fragment and goat anti mouse Alexa Fluor 568 IgG (H+L) were provided by Invitogen and used at 1/1000.

BioID sample preparation

Since we searched for proteins at proximity of the centrosomal pool of FOPNL, we first enriched our sample in centrosomes using isolated centrosome-nucleus complexes (Maro & Bornens, 1980) from HEK293 FlpIn mycBirA*FOPNL and HEK293 FlpIn mycBirA* cells in presence or absence of Tetracycline. BioID purification was then performed according to (Roux *et al*, 2012). Briefly, the purified centrosome-nucleus complexes were then incubated 10 min in 50mM Tris pH 7.4, 300mM NaCl, 0.4% SDS, 5mM EGTA, 1mM DTT, Complete anti- protease cocktail (Roche) then 1% Triton-X-100 were added for 10 min. An equivalent volume of Tris pH 7.4 was added and the lysate was centrifuged à 4°C at 25 000g for 10min at 4°C. The supernatant was collected and incubated overnight with 70 µL of streptavidin beads with gentle agitation at 4°C. Streptavidin beads were washed with 50mM Tris pH7.4. After the last wash, the proteins were recovered from the beads using Laemmli sample buffer. Proteins were allowed to enter the SDS acrylamide gel for 1cm. Gels were stained using colloidal blue. The gel containing the proteins is then cut (gel plug).

Samples preparation prior to LC-MS/MS analysis

Gel plugs were discolored using a solution of ACN/NH_4HCO_3 50mM (50/50) during 15 min with agitation. Plugs were reduced with a solution of 10 mM DL-Dithiothreitol (DTT, Sigma-Aldrich, Saint Louis, MO, USA) during 45 min at 56°C, then the plugs were alkylated using à 55mM solution of Iodoacetamide (IAA, Sigma-Aldrich, Saint Louis, MO, USA) during 45 min at room temperature. After a step of washing and dehydration, proteins in the plugs where digested overnight with Trypsin (10µg/ml) (Promega, Madison, WI, USA) at 37°C in a 25-mM NH_4HCO_3 buffer (0.2 µg trypsin in 20 µL). The resulting peptides were desalted using ZipTip µ-C18 Pipette Tips (Pierce Biotechnology, Rockford, IL, USA).

LC-MS/MS acquisition

Samples were analyzed using an Orbitrap Fusion equipped with an easy spray ion source and coupled to a nano-LC Proxeon 1200 (Thermo Scientific, Waltham, MA, USA). Peptides were loaded with an online preconcentration method and separated by chromatography using a Pepmap-RSLC C18 column (0.75 x 750 mm, 2 µm, 100 Å) (Thermo Scientific), equilibrated at 50°C and operating at a flow rate of 300 nl/min. Peptides were eluted by a gradient of solvent A (H_2O, 0.1 % FA) and solvent B (ACN/H_2O 80/20, 0.1% FA), the column was first equilibrated 5 min with 95 % of A, then B was raised to 28 % in 105 min and to 40% in 15 min. Finally, the column was washed with 95% B during 20 min and re-equilibrated at 95% A during 10 min. Peptide masses were analyzed in the Orbitrap cell in full ion scan mode, at a resolution of 120,000, a mass range of *m/z* 350-1550 and an AGC target of 4.10^5. MS/MS were performed in the top speed 3s mode. Peptides were selected for fragmentation by Higher-energy C-trap Dissociation (HCD) with a Normalized Collisional Energy of 27% and a dynamic exclusion of 60 seconds. Fragment masses were measured in an Ion trap in the rapid mode, with and an AGC target of 1.10^4. Monocharged peptides and unassigned charge states were excluded from the MS/MS acquisition. The maximum ion accumulation times were set to 100 ms for MS and 35 ms for MS/MS acquisitions respectively.

Data analysis

Label-free quantification was done on Progenesis QI for Proteomics (Waters, Milford, MA, USA) in Hi-3 mode for protein abundance calculation. MGF peak files from Progenesis were processed by Proteome Discoverer 2.2 with the Mascot search engine (Matrix Science, version 2.4). Identification of proteins was done with the Swissprot database release 2018_12 with the *Homo sapiens* taxonomy. A maximum of 2 missed cleavages was authorized. Precursor and fragment mass tolerances were set to respectively 7 ppm and 0.5 Da. The following post-translational modifications were included as variable: Acetyl (Protein N-term), Oxidation (M), Phosphorylation (STY), D-Biotin (K). The following post-translational modifications

were included as fixed: Carbamidomethyl (C). Spectra were filtered using a 1% FDR using the percolator node.

CEP90 gene identification in Paramecium

By BLAST search in Parameciumdb (https://paramecium.i2bc.paris-saclay.fr/), we identified two *Paramecium* genes encoding proteins homologous to CEP90: *CEP90a* (PTET.51.1.G0320241) and CEP90b (PTET.51.1.G0320283) (Arnaiz *et al*, 2020). CEP 90a and b protein shares about 20,7% identity with human CEP90 protein. These two genes result from the last whole genome duplication, which occurred in *Paramecium*, and share 95,2% identity. RNAseq analysis as well as microarray show that CEP90a is 10x more expressed than CEP90b.

Genes cloning

For gene silencing, the more divergent part of the gene was chosen to selectively inactivate either *CEP90a* or *CEP90b*, since the two paralogs of *CEP90* in *Paramecium* share a high percentage of identity. A 479bp fragment (bp 1472-1951 from ATG start codon) from *CEP90a* gene and a 501bp (bp 1399-1900 from ATG start codon, see Table S2) fragment from *CEP90b* were amplified by PCR and cloned into the appropriate sites of the L4440 vector. This vector allows the synthesis of double-stranded RNA corresponding to the cloned gene from two T7 promoters. The possible off-target effect of this sequence was analyzed using the RNAi off-target tool in the *P. tetraurelia* genome database (https://paramecium.i2bc.paris-saclay.fr/cgi/tool/rnai_off_target) that searches the genome for stretches of 23 identical nucleotides (the size of *Paramecium* siRNA). The only genomic sequence matching for *CEP90a* and *CEP90b* RNAi fragment were *CEP90a* or *b*, thus ruling out possible off-targeting. The inactivation of both CEP90a and CEP90b was performed using a L4440 vector containing the same *CEP90a* fragment (1472-1951) linked to a new fragment of *CEP90b* (139-618 from ATG start codon). Since the 139-618 *CEP90b* fragment is localized in a less divergent part, an OFF-Target effect has been identified on CEP90a with a hit of 3.

Silencing vectors of FOPNL, OFD1, PtCen2 and PtCen3 have already been described previously(Aubusson-Fleury *et al*, 2012), (Bengueddach *et al*, 2017), (Ruiz *et al*, 2005).

For CEP90-GFP expression, *CEP90a* gene showing a 10x higher expression level than *CEP90b* gene during the vegetative state of *Paramecium*, *CEP90a* gene was chosen for expressing the GFP-tagged fusion protein. A synthetic *CEP90a* gene, resistant to *CEP90a* RNAi vector was designed by punctual modifications (from base 1472 to 1951 from the ATG start codon). Both wild type and RNAi resistant constructions were inserted in PPXV-GFP plasmids. As a result, the GFP is fused in the C-terminus of *CEP90a* and RNAi resistant *CEP90a* gene. The fusion proteins are expressed under the control of the calmodulin promoter.

Human cDNA of FOPNL (provided by O. Rosnet) was amplified by PCR using primers (Table S2) and cloned into pcDNA5 FRT/TO mycBirA* using the appropriate restriction sites.

Generation of stable and inducible HEK293 flpIn FOPNL for BioID

Flp-In T-REx HEK293 cells were cotransfected with pOG44 (Flp-recombinase expression vector) and either pcDNA5FRT/TO mycBirA*FOPNL or pcDNA5FRT/TO. Transfections were performed with Lipofectamine2000 according to the manufacturer's instructions. After transfection, cells were selected with hygromycin (200µg/mL) and blasticidin (15µg/mL). HEK293 FlpIn mycBirA*FOPNL and HEK293 FlpIn mycBirA* cells were incubated for 24 h with 50 µM biotin (Sigma-Aldrich) in the presence or absence of 0.1 µg/ml tetracycline.

Paramecium transformation

Nd7-1 cells were transformed by microinjection into their macronucleus (Gilley *et al*, 1988). DNA containing a mixture of the plasmid of interest (*CEP90-GFP*, *CEP90RNAi resistant GFP*, *OFD1-GFP*, *GFP-FOPNL* at 5 µg/µl) with the DNA directing the expression of the *ND7* gene to complement the *Nd7* mutation. Microinjection was made under an inverted Nikon phase-contrast microscope, using a Narishige

micromanipulation device and an Eppendorf air pressure microinjector. Transformants were screened for their ability to discharge their trichocysts and further analyzed for GFP. Clones expressing the fusion protein and showing a growth rate similar to untransformed paramecia were chosen for further analyses.

Gene silencing in Paramecium by feeding

L4440 inactivation vectors were transformed in HT115 DE3 Escherichia coli strain to produce T7Pol-driven dsRNA as previously described (Galvani & Sperling, 2002). Paramecia were fed with these bacteria and refed daily with a fresh feeding medium at 27°C. Control cells were fed with HT115 bacteria carrying the L4440 vector containing the *ND7* gene (control). Phenotypes were analyzed after 48h of feeding. In these conditions, most of the mRNA of silenced genes are knocked-down therefore leading to the depletion of the proteins.

Effectiveness of RNAi was quantified by analyzing the decrease of BB fluorescence in transformed cell lines expressing the GFP –tagged transgene after silencing. In *Paramecium*, the phenotype of silenced cells is highly reproducible from one experiment to another and from one cell to another. In each experiment paramecia were analyzed in at least 2 or 3 independent experiments.

Paramecia fixation for immunofluorescence

Fixation and immunofluorescence techniques were performed on cells in suspension. 50-100 cells were collected in the smallest volume possible and were permeabilized in 200 µl PHEM (Pipes 60mM, Hepes 25 mM, EGTA 10mM, MgCl2 2mM, adjusted to pH 6.9) with 1% Triton-X-100 (PHEM-Triton) for 30 secondes. Cells were fixed for 10min in 2% PHEM-PFA. Buffer was then aspirated and cells were rinsed 3 times for 10 min in PBS –tween 0.1%-3% BSA

Confocal acquisition

Confocal acquisitions were made with a Leica SP8 equipped with a UV diode (line 405), and three laser diodes (lines 488, 552 and 635) for excitation and two PMT detectors. For U-ExM data, images were collected with an inverted confocal Microscope Leica DMI 6000 CS (*Paramecium*) or an inverted Leica TCS SP8 microscope (human cells) using a 63 × 1.4 NA oil objective with Lightening mode at max resolution, adaptive as 'Strategy' and water as 'Mounting medium' to generate deconvolved images. 3D stacks were acquired with 0.12 µm z-intervals and an x, y pixel size of 35 nm.

Expansion microscopy- U-ExM

For analyzing CEP90 and OFD1 in human centrioles, U-ExM was performed as previously described (Steib *et al*, 2020). The following reagents were used in U-ExM experiments: formaldehyde (FA, 36.5–38%, F8775, SIGMA), acrylamide (AA, 40%, A4058, SIGMA), N,N'-methylenbisacrylamide (BIS, 2%, M1533, SIGMA), sodium acrylate (SA, 97–99%, 408220, SIGMA), ammonium persulfate (APS, 17874, ThermoFisher), tetramethylethylendiamine (TEMED, 17919, ThermoFisher), nuclease-free water (AM9937, Ambion-ThermoFisher) and poly-D-Lysine (A3890401, Gibco). Briefly, coverslips were incubated in 2% AA + 1.4% FA diluted in PBS for 5 hr at 37°C prior to gelation in monomer solution (19% sodium acrylate, 0.1% BIS, 10% acrylamide) supplemented with TEMED and APS (final concentration of 0.5%) for 1 hr at 37°C and denaturation for 1h30 min at 95°C, gels were stained for 3 hr at 37°C with primary antibodies :CEP90 or OFD1 and a combination of tubulin monobodies (see antibodies section) diluted in homemade PBS-BSA 2%. After 3 PBS-tween 0.1% washes, secondary antibodies were incubated for 2h30 min at 37°C. Gels were then washed 3 times in PBS-tween 0.1% and incubated in water overnight to allow expansion.

For *Paramecium* BB expansion microscopy, the following modification has been done: purified cortex was incubated in 1%AA + 0.5%FA diluted in 1XPBS for 5h at 37°C. The GFP-tagged proteins were stained with Rabbit anti-GFP (1/400 Torrey Pines TP-401) and the combination of tubulin monobodies as above.

Electron microscopy

For ultrastructural observations, cells were fixed in 1% (v/v) glutaraldehyde and 1% OsO4 (v/v) in 0.05 M cacodylate buffer, pH 7.4 for 30 min. After rinsing, cells were embedded in 2% agarose. Agarose blocks were then dehydrated in graded series of ethanol and propylene oxide and embedded in Epon812 (TAAB, Aldermaston, Berkshire, UK). For pre-embedding immunolocalization, the immunostaining process was carried out as described for immunofluorescence using gold-coupled instead of fluorochrome-coupled secondary antibodies (gold-labeled anti-rabbit IgG -GAR G10, Aurion) diluted 1/30 for 30 min. Cells were then treated as described above.

All ultrathin sections were contrasted with uranyl acetate and lead citrate. The sections were examined with a Jeol transmission electron microscope1400 (at 120kV).

Paramecium swimming analysis.

4 to 8 paramecia were transferred in 10 µl drops of conditioned BHB (bacterized BHB solution and depleted of bacteria after their growth and sterilized) for 15 min before being tracked for 10s every 0.3s. We used a Zeiss Steni 2000-C dissecting microscope with a Roper Coolsnap-CF camera and Metamorph software (Universal Imaging). Stacks were analyzed using the Manual tracking tool in ImageJ.

Mammalian cell fixation and immunofluorescence

RPE1 cells were grown on coverslips, washed in PBS, and fixed in methanol at -20°C for 6 min. Alternatively, after a PBS wash, cells were extracted in a PHEM buffer (45 mM Pipes, 45 mM Hepes, 10 mM EGTA,5 mM MgCl2 adjusted to pH 6.9, and 1 mM PMSF) containing 1% TritonX-100 and then fixed as described above. Cells were rinsed in PBS containing 0.1% Tween 20. Primary antibodies diluted in PBS containing 3%BSA were added for 1 h at room temperature. Three washes were per-formed in PBS-Tween, and the Alexa-labeled secondary antibodies were applied (FisherScientific)).Cells were washed in ethanol and mounted in Citifluor (CityUniversity, London, England). Observations were done on a confocal

microscope. All documents presented are two-dimensional projections of images collected at all relevant z-axes

siRNA-mediated protein depletion

30000 RPE1 cells were plated onto coverslips 24 hr prior transfection. For CEP90 depletion, two siRNA were synthesized. One is a smart pool of Dharmacon and the other one corresponding to nucleotides 1651-1675 and used in the Kodani's paper (Kodani *et al*, 2015). Similarly, two siRNA were used for FOPNL. One is a smart pool of Dharmacon and the other one the published siRNA sequence (Sedjaï *et al*, 2010) as well as a smart pool of Dharmacon. Scrambled siRNA was used as a negative control. Cells were transfected with 20nM of siRNA using Lipofectamine RNAiMax (Invitrogen). Medium was changed 4 hr post-transfection and cells were analyzed 48 hr post-transfection.

Image analysis

For immunofluorescence, image stacks were processed with ImageJ and Photoshop. Confocal acquisition parameters were kept identical (same laser intensity and same gain and same resolution) for quantification of BB fluorescence intensity in control and RNAi treated cells. Mean pixel fluorescence intensity of the different antibodies was then measured within a defined and constant circular area of the size of the BB (*Paramecium*) or centrosome (RPE1 cells), using the measurement tools of ImageJ.

For U-ExM data acquisition of Paramecium cortex, confocal images were acquired with a LEICA TCS SP8x (DMi 6000) equipped with a 63x Apochromat oil-immersion objective (numerical aperture (NA): 1.4), U.V diode laser 405nm and a white light laser (WLL) AOTF coupled. Excitation at 490nm and 571nm of Alexa 488 and Alexa 568, respectively. Images were recorded with two hybrid detectors. Acquistions were made at 512x512 pixels and 400Hz speed and zoom of 8.4. Alexa 488 was acquired with a frame accumulation of 3. Sample sampling was 43nm in XY and for 3D imaging, stacks were acquired with a z-step of 130nm. The whole system was driven by LAS X software version 3.5.6. Image manipulation were done with ImageJ (Wayne Rasband, National Institutes of Health). Images were deconvolved employing

the Huygens Essential package (Scientific Volume Imaging, Hilversum, The Netherlands), with sampling of 43nm in XY and 130nm in Z and the following parameters: algorithm : CMLE; signal/noise ratio : 20; quality threshold : 0.01%; maximum iterations : 40; background calculation : in/near objects.

For U-ExM analysis, length coverage and diameter quantification was performed as previously published in (Steib *et al*, 2020b).

To generate the panels in Figure 1I, 5I, 5J and S1F, two homemade plugins for ImageJ were used. The first one helps the user to easily pick the extremities of a centriolar protein signal. For each protein of each image, the user picks the first and the last point of the signal along the centriole length. This generates an entry in a table for each centriole describing where the proteins start and end. The results are saved in a .csv file that can be directly read by the second plugin. The second plugin reads the table generated by the first plugin and summarizes the positions of different proteins in one plot. For each centriole, one protein (here the tubulin) is defined as the reference protein and its Y coordinates are shifted so its Y starting point is set to 0. The same shift is applied to the second protein to keep the correct distances between the 2 proteins. The Y coordinates values of both signals are then rescaled to the average length of the reference protein. For each protein, the average and side deviation of the Y starting position and of the Y ending position is calculated. A plot is then generated illustrating the average position of one protein to the other.

Statistical analysis

The statistical significance of the difference between groups was determined using one-way ANOVA followed by Tukey's post hoc test. All data are presented as mean +/- SEM as specified in the figure legends. Differences were considered significant when $p<0.05$. Results reported are from 2-3 independent biological replicates as noted in legends with reproducible findings each time.

Acknowledgements:
We would like to thank Carsten Janke for his generous gift of anti-poly-E antibodies. We acknowledge Mireille Bétermier and all members of the Bétermier lab and Tassin lab for stimulating discussions. We thank B. Durand for critical reading of the manuscript. We thank Cindy Mathon for maintaining the Paramecium cell cycle and her great help in molecular biology and immunofluorescence staining and Pascaline Tirand for excellent technical assistance. The present work has benefited from Imagerie-Gif core facility supported by I'Agence Nationale de la Recherche (ANR-11-EQPX-0029/Morphoscope, ANR-10-INBS-04/FranceBioImaging; ANR-11-IDEX-0003-02/ Saclay Plant Sciences). This work has been founded by basal body anchoring in ciliogenesis: structure-function analysis: ANR-15-CE11-0002-01 to AMT. PLB was supported by PhD fellowships from Universite´ Paris-Saclay (https://www.paris-saclay.fr/). This work has been supported by the Fondation ARC pour la recherche sur le cancer" to PLB ARCDOC4202003000178 and by the Swiss National Science Foundation (SNSF) PP00P3_187198 and by the European research Council ERC ACCENT StG 715289 attributed to Paul Guichard.

Author contributions

AMT conceived, supervised, designed the project, and wrote the final manuscript with input from all authors. PLB, performed almost all experiments, image acquisition, processing and analyzed the data. ML performed ultrastructure expansion on mammalian cells, images acquisition and analyzed and quantified all U-ExM data. LG performed the first mammalian siRNA experiments; ML performed the electron microscopy of *Paramecium*. MLG wrote the U-ExM quantification ImageJ PlugIn. OR provided antibodies and cell lines. LL and GC performed mass spectrometry analysis. MT acquired with PLB the *Paramecium* U-ExM confocal images. FK, VH and PG performed formal analysis, review and editing.

Conflict of interest
The authors have declared that no competing interests exist**.**

Figures legends:

Main

Figure 1: Localization of CEP90 GFP, GFP-FOPNL and OFD1-GFP In *Paramecium*.

A-B': Labelling of CEP90-GFP (A, B) and GFP-FOPNL (C,D) paramecia transformants using the polyclonal anti-polyglutamylated tubulin antibodies (Poly-E, magenta). A, B: Projection of confocal sections through the ventral surface. On the ventral side (A, B), the green emitted fluorescence of GFP overlapped with the anti-poly-E labeling on all basal bodies, as shown on the magnification on the right panel. Scale bars= 20 µm and 2 µm (magnification). A', B': Projection of confocal sections at the intracytoplasmic level. BB at the cell surface showed that the GFP signal (green) is located at the distal part of all basal bodies (magenta) underneath the epiplasm (orange) for both CEP90-GFP and GFP-FOPNL. Scale bars= 20 µm and 1.7 µm (magnification)

C-G: Cortex from transformants expressing CEP90-GFP, OFD1-GFP and GFP-FOPNL were purified and expanded using the U-ExM technique. Gullet cortical fragments displaying ciliated BB were selected since U-ExM gave better results in this region. Anti-GFP antibodies (green) and anti-tubulin mixed antibodies (magenta) (see material and methods) were used to label respectively the fusion protein and the BB microtubule wall. C-E': Labeling of the fusion protein on BB observed longitudinally (upper panel) or top view (lower panel). CEP90-GFP (C), OFD1-GFP (D) and GFP-FOPNL (E) BB display the GFP staining close to the microtubule wall of the BB (magenta) and slightly underneath the distal end staining of the anti-tubulin signal. Top view images demonstrate that the GFP signal is organized in a 9-fold symmetry (C',D', E'). Scale bar= 100nm. The distance to the proximal end (F) and microtubule wall (G) were quantified and statistically analyzed (***$p<0.0001$, one-way ANOVA followed by Tukey's post hoc test).

N= 14 (CEP90), 15 (FOPNL), 9 (OFD1) BB from 2 independent experiment. Average +/- SD: CEP90= 418.4 +/- 21.7 nm ;FOPNL=430.6 +/- 62.6 nm; OFD1=432.3 +/- 29.9 nm.

H-J: Representative EM images of the immunolocalization of CEP90-GFP protein on BB revealed by anti-GFP antibodies. H-I: longitudinal view (H) and transverse sections of BBs at the level of the intermediate plate (I). Note that gold particle are located close to the transition zone or at the level of the intermediate plate Scale bar= 100nm. J: BB diagrams recapitulating the localization of gold beads in the 5 different zones indicated (1-5). Quantification of gold particle number counted on 35 BB in 2 independent experiments. Note that the majority of the beads were localized at the transition zone level between the axosomal plate and the terminal plate, known to be the place where the transition fibers emerge from the microtubule doublet.

Figure 2: CEP90 depletion affects basal body docking

A: Projection of optical sections through the ventral surface (A) labeled with polyE antibodies (grey) in control (Ctrl) RNAi, CEP90 RNAi and FOPNL RNAi *Paramecium*. A': Projection of confocal sections at the intracytoplasmic level labeled with poly-E antibodies (grey) in Ctrl RNAi and *CEP90* RNAi and *FOPNL* RNAi. In control-depleted cells, basal bodies are organized in parallel longitudinal rows highlighted in the magnification (right panel) (A) with no BB observed in the cytoplasm (A'). Cells observed after 2 divisions upon CEP90 or FOPNL depletion appear smaller than control ones, with a severe disorganization of the basal body pattern (A). Numerous internal basal bodies are observed in the cytoplasm (A'). Scale bars= 20 µm and 2 µm (magnification).

B-C: Specificity of CEP90 RNAi. Transformants expressing either WT CEP90-GFP (B) or a RNAi resistant CEP90-GFP (C) were observed after 2-3 divisions upon CEP90 depletion and analyzed for green emitted fluorescence and BB staining using poly-E antibodies. Scale bars= 20µm and 2 µm (magnification). B: The green fluorescence (green) of WT CEP90-GFP transformants was severely reduced along with the expected

disorganisation of BB at the cell surface. C: By contrast the expression of an RNAi-resistant CEP90-GFP rescued endogenous CEP90 depletion and restored the cortical organization of BB.

Figure 3: CEP90 depletion affects basal body's distal end maturation

A: *Paramecium* showing one BB unit with a ciliated after control RNAi depletion (Ctrl). The TZ is characterized by three plates indicated by colored arrowheads: terminal plate (green), intermediate plate (blue) and axosomal plate (magenta). B-D: Upon CEP90 depletion, undocked basal bodies are detected close to the cell surface (C, E) or deep in the cytoplasm (B, D). Vestigial structures resembling the axosomal plate (magenta arrowhead) and intermediate plate (blue) are detected on all internal BB (63 examined). E: Some BB display microtubule extensions on the free, uncapped side of the basal body (white arrow). Scale bar= 200nm.

Figure 4: Sequential recruitment of basal body anchoring proteins in *Paramecium*.

(A) *Paramecium* transformants expressing either Cen2-GFP, CEP90-GFP or OFD1-GFP (green) have been stained for basal bodies (poly-E antibodies magenta) after 2 or 3 divisions in control cells (Ctrl) and upon OFD1, CEP90 and FOPNL depletion. Control depleted paramecia displayed well anchored basal bodies organized in parallel longitudinal rows, with the GFP emitted signal overlapping BB labeling. After OFD1, CEP90 and FOPNL depletion, BB disorganization is observed. The depletion of either OFD1, CEP90, or FOPNL does not affect Cen2-GFP recruitment to BB, as determined by the colocalization of GFP signal and poly-E staining which appear in white. In contrast, depletion of OFD1, CEP90 and FOPNL on CEP90 or OFD1 transformants prevents the recruitment of the fusion protein to the newly formed BB. The BB appear in magenta instead of white on control depleted cells (white arrowheads). Scale bars= 20µm and 2µm (magnification). B-D: Quantification of the GFP fluorescence of CEP90-GFP (B), Cen2-GFP (C) and OFD1-GFP (D) on newly formed basal body in Control and upon Cen2, OFD1, CEP90, FOPNL and Cen3 depletions. Dot plot showing the mean percentage of GFP fluorescence (n= 80 cells, 3 independent replicates), error bars show SEM. Statistical significance was assessed by one-way ANOVA followed by

Tukey's post hoc test p<0.0001 ****. E: Schematic representation of the sequential recruitment of basal body anchoring proteins leading to proper maturation of BB distal end. Cen2 arrives first at the BB followed by the interdependent recruitment of FOPNL, CEP90 and OFD1. This functional ternary complex is required to allow Cen3 recruitment and basal body docking.

Figure 5: Centrosomal localization of CEP90 and OFD1 in mammalian cells

A, B: RPE1 cells were stained with the mouse monoclonal GT335 antibody directed against tubulin polyglutamylation (centrioles magenta) and rabbit anti-CEP90 (green) (A) or rabbit anti-OFD1 (cyan) (B). Both CEP90 and OFD1 decorated the centrosome and the centriolar satellites. Scale bar= 5µm C-H: U2OS cells were expanded using the U-ExM technique stained for tubulin (magenta) and CEP90 (green) or OFD1 (cyan). C,D, F,G Longitudinally oriented S phase centrosomes, stained with CEP90 (C,D) and OFD1(F,G) antibodies. Note that both CEP90 and OFD1 are localized slightly underneath the distal end of both the mother (MC) as well as the procentrioles (PC). E,H: top view of a mother centriole showing the 9-fold symmetry organization of CEP90 and OFD1 at the distal end of the centriole. Scale bar= 200nm. I: Distance between the proximal part of centriole (tubulin) and the maximal intensity of CEP90 (green) or OFD1 (cyan). N=23 and 25 centrioles from 3 independent experiments. Average +/- SD : CEP90= 364.4 +/- 17.3 nm, OFD1 = 370.3 +/- 16.9 nm. J: Angle measured between two following dots CEP90 or OFD1 fluorescent dots and the center of the centriole (on top view). N= 16 (CEP90) and 14 (OFD1) centrioles from 3 independent experiment. Average +/- SD: CEP90=41.7 +/- 1.3°; OFD1=40.7 +/- 2.9°. J: Distance between the maximal intensity of tubulin and the maximal intensity of CEP90 (green) or OFD1 (cyan) based on 22 (CEP90) and 18 (OFD1) centrioles from 3 independent experiments. Average +/- SD: CEP90= 31.4 +/- 4.2 nm, OFD1 = 42.7 +/- 5.9 nm . K: Localization of CEP90 and OFD1 with respect to the microtubule wall. Note that OFD1 localizes more externally than CEP90.

Figure 6: FOPNL and CEP90 regulate distal appendage proteins recruitment in mammalian cells.

A: CEP90, FOPNL, OFD1 and distal appendage proteins (CEP83, CEP89, and CEP164) were examined in control siRNA (Ctrl), FOPNL siRNA and CEP90siRNA in RPE1 cells by IF after 24h of serum-starvation using the indicated antibody. Scale bar= 5µm. B-G: quantification of the fluorescence intensity of antibodies: FOPNL (B), CEP90 (C), OFD1 (D), CEP83 (E), CEP89 (F) and CEP164 (G) staining at the centrosome. All data are presented as mean ± SD. ****$p < 0.001$ (one-way ANOVA followed by Tukey's post hoc test), $n \geq 60$ centrosomes in 2/3 independent experiment.

Figure 7: diagram of the function of the CEP90, FOPNL and OFD1 in distal appendages assembly

During centriole duplication the ternary complex composed of CEP90, FOPNL and OFD1 is recruited on the two procentrioles at the distal extremity position, which is correlated with the position of distal appendages. During G2/M the procentrioles elongate maintaining the ternary complex distally. The ancient daughter centriole matures in a mother one, by losing DCP and assembling distal appendages. When one of the protein of this complex (CEP90, FOPNL, and OFD1) is depleted, none of these proteins is recruited to the centriolar wall leading to defective distal end appendage assembly and defective ciliogenesis. We propose that this complex is required to specify on the procentriole the future location of distal appendage assembly.

Supplementary material:

Table S1: myc-BirA*-FOPNL BioID raw protein measurement.

MS/MS comparison of two biological replicates of the myc-BirA*-FOPNL with the myc-BirA*. High-confidence interactors were defined as those with q value <0.05 and max fold >2.

Table S2: Primer, RNAi, siRNA and CEP90-GFP RNAi-resistant sequences. All primers used to construct *Paramecium* CEP90-GFP and CEP90-GFP resistant plasmid as well as *CEP90a* and *CEP90b* gene silencing vectors were synthesized by Eurofins Genomics. The RNAi-resistant sequence of CEP90-GFP RNAi-resistant plasmid (red) was designed following the ciliated codon code and

was synthesized by Integrated DNA technologies. siRNA sequences directed against CEP90 and FOPNL were synthesized by Dharmacon according to the manufacturer's protocol. In both case a published single sequence were used (siRNA CEP90 #2 and siRNA FOPNL #1) as well as a combination of 4 sequences directed against the gene (smartpool).

Figure S1: Localization of CEP90-GFP, OFD1-GFP and GFP-FOPNL by U-ExM

A: EM on *Paramecium* cortex fragment showing a two-BB unit. During cortex purification, cilia shed above the transition zone (white arrowhead). The unciliated BB (yellow arrowhead) remain unmodified. Scale bar= 100 nm. B-E: U-ExM performed on paramecia transformant expressing CEP90-GFP (B), OFD1-GFP (C) and GFP-FOPNL (D, E) show BB and cilia stained with tubulin antibody (magenta). Note that a space indicated by a white arrowhead shows the cilium breakage between the distal end of the TZ and the cilium. B, C: CEP90-GFP and OFD1-GFP signal are localized at the distal extremity of non-ciliated BB (yellow arrowhead) while GFP signal is slightly underneath the distal end of ciliated BB (white arrowhead). Scale bar= 250 nm. F: Schematic representation of OFD1 (blue square), FOPNL (orange square) and CEP90 (green square) localization on ciliated and unciliated basal bodies.

Figure S2: CEP90 depletion phenotypes

A,C: *Paramecium* were transformed with a construction expressing either WT CEP90-GFP or a RNAi-resistant CEP90-GFP. A: BB GFP signal fluorescence has been quantified on newly formed basal bodies (anterior ones) after 2/3 division upon CEP90 depletion. mean ± SD is represented, ****$p < 0.001$ (one-way ANOVA followed by Tukey's post hoc test), $n \geq 60$ basal bodies on 2 independent experiments. B: cells compared to control depleted cells. Note that both CEP90 and FOPNL depleted cells died after 4 or 5 divisions. C: Dot plot graph depicting the mean swimming speeds of non-injected paramecia (NI), paramecia expressing WT CEP90-GFP or RNAi-resistant CEP90-GFP after 48h under control condition or CEP90 RNAi condition. Each dot shows the mean velocity of 1 cell, mean ± SD is represented, ****p<

0.001 (one-way ANOVA followed by Tukey's post hoc test, $n \geq 120$ cells per condition performed in 2 independent replicates).

Figure S3: CEP90 depletion does not affect BB duplication

Early to middle stage of *Paramecium* division decorated with poly-E antibodies (grey). In the ventral side of the cell at an early stage of division, a new oral apparatus assembles. On both sides of the future fission line, basal body duplication takes place. The first division of paramecia was observed after control (Ctrl), CEP90 or FOPNL depletion. No significant duplication defects have been observed after FOPNL or CEP90 depletion. Scale bars= 20µm and 2 µm (magnification)

Figure S4: Recruitment of CEN2-GFP, CEP90-GFP, OFD1 GFP and GFP-FOPNL in Cen2, Cen3 and CEP90 depleted cells to newly formed BB

A: Transformants expressing a GFP-tagged FOPNL were observed 2-3 divisions upon control (Ctrl) or CEP90 depletion. GFP-FOPNL fluorescence (green) was severely reduced on newly formed basal bodies along with the expected basal body disorganization. Scale bar= 20µm. B: Dot plots showing the mean percentage of GFP-FOPNL BB fluorescence after 2-3 divisions in either FOPNL or CEP90 RNAi ($n \geq 100$ basal bodies per condition performed in 2 independent replicates), error bars show SEM. Statistical significance was assessed by a one-way ANOVA followed by Tukey's post hoc test $p<0.0001$ ****. C-D: *Paramecium* transformants expressing Cen2-GFP, CEP90 GFP or OFD1-GFP (green) have been stained for basal bodies (poly-E antibodies, magenta) after 2-3 divisions upon Cen2 (C) or Cen3 (D) depletion. After Cen2 and Cen3 depletion, BB disorganisation is observed. C: The GFP fluorescence is not recruited to newly formed BB after Cen2 RNAi. D: By contrast, Cen3 depletion did not affect neither CEP90-GFP, OFD1-GFP and GFP-FOPNL recruitment to BB. Scale bars= 20µm and 2 µm (magnification).

Figure S5 :Colocalization of FOPNL and CEP90 in HeLA cells and ciliogenesis defects

A: HeLa-Kyoto cell lines expressing GFP-FOPNL (green) were stained for CEP90 (magenta). Confocal images show the colocalization of both proteins at centrosome and centriolar satellites. Scale bar= 5µm. B: Serum-starved RPE1 during 24h were stained for cilia with GT335 in control (Ctrl), CEP90 or FOPNL siRNA. Percentage of ciliated cells were quantified in each condition. mean ± SD is represented, ****$p < 0.001$ (one-way ANOVA followed by Tukey's post hoc test, $n \geq 350$ cells per condition performed in 3 independent replicates).

Figure S6: **Effect of CEP90 and FOPNL depletion on the daughter centriolar protein, Centrobin**

The daughter centriolar protein Centrobin was localized in control (Ctrl), CEP90 and FOPNL depleted RPE1 cells. No significant differences are observed between control-depleted cells and CEP90 or FOPNL depleted cells. Scale bar= 5µm

Bibliography

Adoutte A, Ramanathan R, Lewis RM, Dute RR, Ling KY, Kung C & Nelson DL (1980) Biochemical studies of the excitable membrane of Paramecium tetraurelia. III. Proteins of cilia and ciliary membranes. *J Cell Biol* 84: 717–738

Arnaiz O, Goût J-F, Bétermier M, Bouhouche K, Cohen J, Duret L, Kapusta A, Meyer E & Sperling L (2010) Gene expression in a paleopolyploid: a transcriptome resource for the ciliate Paramecium tetraurelia. *BMC Genomics* 11: 547

Arnaiz O, Meyer E & Sperling L (2020) ParameciumDB 2019: integrating genomic data across the genus for functional and evolutionary biology. *Nucleic Acids Res* 48: D599–D605

Aubusson-Fleury A, Lemullois M, de Loubresse NG, Laligné C, Cohen J, Rosnet O, Jerka-Dziadosz M, Beisson J & Koll F (2012) The conserved centrosomal protein FOR20 is required for assembly of the transition zone and basal body docking at the cell surface. *J Cell Sci* 125: 4395–4404

Aury J-M, Jaillon O, Duret L, Noel B, Jubin C, Porcel BM, Ségurens B, Daubin V, Anthouard V, Aiach N, *et al* (2006) Global trends of whole-genome duplications revealed by the ciliate Paramecium tetraurelia. *Nature* 444: 171–178

Azimzadeh J, Hergert P, Delouvée A, Euteneuer U, Formstecher E, Khodjakov A & Bornens M (2009) hPOC5 is a centrin-binding protein required for assembly of full-length centrioles. *J Cell Biol* 185: 101–114

Bengueddach H, Lemullois M, Aubusson-Fleury A & Koll F (2017) Basal body positioning and anchoring in the multiciliated cell Paramecium tetraurelia: roles of OFD1 and VFL3. *Cilia* 6: 6

Bowler M, Kong D, Sun S, Nanjundappa R, Evans L, Farmer V, Holland A, Mahjoub MR, Sui H & Loncarek J (2019) High-resolution characterization of centriole distal appendage morphology and dynamics by correlative STORM and electron microscopy. *Nat Commun* 10: 993

Chang C-W, Hsu W-B, Tsai J-J, Tang C-JC & Tang TK (2016) CEP295 interacts with microtubules and is required for centriole elongation. *J Cell Sci* 129: 2501–2513

Chevrier V, Bruel A-L, Van Dam TJP, Franco B, Lo Scalzo M, Lembo F, Audebert S, Baudelet E, Isnardon D, Bole A, *et al* (2016) OFIP/KIAA0753 forms a complex with OFD1 and FOR20 at pericentriolar satellites and centrosomes and is mutated in one individual with oral-facial-digital syndrome. *Hum Mol Genet* 25: 497–513

Dupuis-Williams P, Fleury-Aubusson A, de Loubresse NG, Geoffroy H, Vayssié L, Galvani A, Espigat A & Rossier J (2002) Functional role of epsilon-tubulin in the assembly of the centriolar microtubule scaffold. *J Cell Biol* 158: 1183–1193

Dute R & Kung C (1978) Ultrastructure of the proximal region of somatic cilia in Paramecium tetraurelia. *J Cell Biol* 78: 451–464

Failler M, Gee HY, Krug P, Joo K, Halbritter J, Belkacem L, Filhol E, Porath JD, Braun DA, Schueler M, *et al* (2014) Mutations of CEP83 cause infantile nephronophthisis and intellectual disability. *Am J Hum Genet* 94: 905–914

Galvani A & Sperling L (2002) RNA interference by feeding in Paramecium. *Trends Genet TIG* 18: 11–12

Gambarotto D, Hamel V & Guichard P (2021) Ultrastructure expansion microscopy (U-ExM). *Methods Cell Biol* 161: 57–81

Gambarotto D, Zwettler FU, Le Guennec M, Schmidt-Cernohorska M, Fortun D, Borgers S, Heine J, Schloetel J-G, Reuss M, Unser M, *et al* (2019) Imaging cellular ultrastructures using expansion microscopy (U-ExM). *Nat Methods* 16: 71–74

Garcia-Gonzalo FR & Reiter JF (2017) Open Sesame: How Transition Fibers and the Transition Zone Control Ciliary Composition. *Cold Spring Harb Perspect Biol* 9

Gheiratmand L, Coyaud E, Gupta GD, Laurent EM, Hasegan M, Prosser SL, Gonçalves J, Raught B & Pelletier L (2019) Spatial and proteomic profiling reveals centrosome-independent features of centriolar satellites. *EMBO J* 38: e101109

Gilley D, Preer JR, Aufderheide KJ & Polisky B (1988) Autonomous replication and addition of telomerelike sequences to DNA microinjected into Paramecium tetraurelia macronuclei. *Mol Cell Biol* 8: 4765–4772

Gogendeau D, Hurbain I, Raposo G, Cohen J, Koll F & Basto R (2011) Sas-4 proteins are required during basal body duplication in Paramecium. *Mol Biol Cell* 22: 1035–1044

Gogendeau D, Lemullois M, Le Borgne P, Castelli M, Aubusson-Fleury A, Arnaiz O, Cohen J, Vesque C, Schneider-Maunoury S, Bouhouche K, *et al* (2020) MKS-NPHP module proteins control ciliary shedding at the transition zone. *PLoS Biol* 18: e3000640

Gonçalves J & Pelletier L (2017) The Ciliary Transition Zone: Finding the Pieces and Assembling the Gate. *Mol Cells* 40: 243–253

Hossain D, Barbelanne M & Tsang WY (2020) Requirement of NPHP5 in the hierarchical assembly of basal feet associated with basal bodies of primary cilia. *Cell Mol Life Sci CMLS* 77: 195–212

Iftode francine, Cohen J, Ruiz F, Torres-Rueda A, Chen-Sban L, Adoutte A & Beisson J (1989) Development of surface pattern during division in Paramecium . I. Mapping of duplication and reorganization of cortical cytoskeletal structures in the wild type. *development* 105: 191–211

Jana SC, Marteil G & Bettencourt-Dias M (2014) Mapping molecules to structure: unveiling secrets of centriole and cilia assembly with near-atomic resolution. *Curr Opin Cell Biol* 26: 96–106

Janke C & Bulinski JC (2011) Post-translational regulation of the microtubule cytoskeleton: mechanisms and functions. *Nat Rev Mol Cell Biol* 12: 773–786

Jeanmaire-Wolf R, Clérot JC, Nahon P, Iftode F, Fleury A & Adoutte A (1993) Isolation and characterization of monoclonal antibodies to cytoskeletal and membrane proteins of the Paramecium cortex. *Eur J Protistol* 29: 311–333

Jerka-Dziadosz M, Gogendeau D, Klotz C, Cohen J, Beisson J & Koll F (2010) Basal body duplication in Paramecium: the key role of Bld10 in assembly and stability of the cartwheel. *Cytoskelet Hoboken NJ* 67: 161–171

Jerka-Dziadosz M, Koll F, Włoga D, Gogendeau D, Garreau de Loubresse N, Ruiz F, Fabczak S & Beisson J (2013) A Centrin3-dependent, transient, appendage of the mother basal body guides the positioning of the daughter basal body in Paramecium. *Protist* 164: 352–368

Joo K, Kim CG, Lee M-S, Moon H-Y, Lee S-H, Kim MJ, Kweon H-S, Park W-Y, Kim C-H, Gleeson JG, *et al* (2013) CCDC41 is required for ciliary vesicle docking to the mother centriole. *Proc Natl Acad Sci U S A* 110: 5987–5992

Kanie T, Abbott KL, Mooney NA, Plowey ED, Demeter J & Jackson PK (2017) The CEP19-RABL2 GTPase Complex Binds IFT-B to Initiate Intraflagellar Transport at the Ciliary Base. *Dev Cell* 42: 22-36.e12

Kim K, Lee K & Rhee K (2012) CEP90 is required for the assembly and centrosomal accumulation of centriolar satellites, which is essential for primary cilia formation. *PloS One* 7: e48196

Kleylein-Sohn J, Westendorf J, Le Clech M, Habedanck R, Stierhof Y-D & Nigg EA (2007) Plk4-induced centriole biogenesis in human cells. *Dev Cell* 13: 190–202

Klotz C, Ruiz F, Garreau de Loubresse N, Wright M, Dupuis-Williams P & Beisson J (2003) Gamma-tubulin and MTOCs in Paramecium. *Protist* 154: 193–209

Knödler A, Feng S, Zhang J, Zhang X, Das A, Peränen J & Guo W (2010) Coordination of Rab8 and Rab11 in primary ciliogenesis. *Proc Natl Acad Sci U S A* 107: 6346–6351

Kobayashi T, Kim S, Lin Y-C, Inoue T & Dynlacht BD (2014) The CP110-interacting proteins Talpid3 and Cep290 play overlapping and distinct roles in cilia assembly. *J Cell Biol* 204: 215–229

Kodani A, Yu TW, Johnson JR, Jayaraman D, Johnson TL, Al-Gazali L, Sztriha L, Partlow JN, Kim H, Krup AL, *et al* (2015) Centriolar satellites assemble centrosomal microcephaly proteins to recruit CDK2 and promote centriole duplication. *eLife* 4: e07519

Kubo A & Tsukita S (2003) Non-membranous granular organelle consisting of PCM-1: subcellular distribution and cell-cycle-dependent assembly/disassembly. *J Cell Sci* 116: 919–928

Kumar D, Rains A, Herranz-Pérez V, Lu Q, Shi X, Swaney DL, Stevenson E, Krogan NJ, Huang B, Westlake C, *et al* (2021) A ciliopathy complex builds distal appendages to initiate ciliogenesis. *J Cell Biol* 220: e202011133

Le Guennec M, Klena N, Gambarotto D, Laporte MH, Tassin A-M, van den Hoek H, Erdmann PS, Schaffer M, Kovacik L, Borgers S, *et al* (2020) A helical inner scaffold provides a structural basis for centriole cohesion. *Sci Adv* 6: eaaz4137

Lopes CAM, Prosser SL, Romio L, Hirst RA, O'Callaghan C, Woolf AS & Fry AM (2011a) Centriolar satellites are assembly points for proteins implicated in human ciliopathies, including oral-facial-digital syndrome 1. *J Cell Sci* 124: 600–612

Lopes CAM, Prosser SL, Romio L, Hirst RA, O'Callaghan C, Woolf AS & Fry AM (2011b) Centriolar satellites are assembly points for proteins implicated in human ciliopathies, including oral-facial-digital syndrome 1. *J Cell Sci* 124: 600–612

Maro B & Bornens M (1980) The centriole-nucleus association: Effects of cytochalasin B and nocodazole. *Biol Cell*: 287–290

Mennella V, Agard DA, Huang B & Pelletier L (2014) Amorphous no more: subdiffraction view of the pericentriolar material architecture. *Trends Cell Biol* 24: 188–197

Mitchison HM & Valente EM (2017) Motile and non-motile cilia in human pathology: from function to phenotypes. *J Pathol* 241: 294–309

Nizak C, Martin-Lluesma S, Moutel S, Roux A, Kreis TE, Goud B & Perez F (2003) Recombinant antibodies against subcellular fractions used to track endogenous Golgi protein dynamics in vivo. *Traffic Cph Den* 4: 739–753

Paintrand M, Moudjou M, Delacroix H & Bornens M (1992) Centrosome organization and centriole architecture: their sensitivity to divalent cations. *J Struct Biol* 108: 107–128

Paoletti A, Moudjou M, Paintrand M, Salisbury JL & Bornens M (1996) Most of centrin in animal cells is not centrosome-associated and centrosomal centrin is confined to the distal lumen of centrioles. *J Cell Sci* 109 (Pt 13): 3089–3102

Reiter JF, Blacque OE & Leroux MR (2012) The base of the cilium: roles for transition fibres and the transition zone in ciliary formation, maintenance and compartmentalization. *EMBO Rep* 13: 608–618

Roux KJ, Kim DI, Raida M & Burke B (2012) A promiscuous biotin ligase fusion protein identifies proximal and interacting proteins in mammalian cells. *J Cell Biol* 196: 801–810

Ruiz F, Beisson J, Rossier J & Dupuis-Williams P (1999) Basal body duplication in Paramecium requires gamma-tubulin. *Curr Biol CB* 9: 43–46

Ruiz F, Garreau de Loubresse N, Klotz C, Beisson J & Koll F (2005) Centrin deficiency in Paramecium affects the geometry of basal-body duplication. *Curr Biol CB* 15: 2097–2106

Ruiz F, Krzywicka A, Klotz C, Keller A, Cohen J, Koll F, Balavoine G & Beisson J (2000) The SM19 gene, required for duplication of basal bodies in Paramecium, encodes a novel tubulin, eta-tubulin. *Curr Biol CB* 10: 1451–1454

Schmidt KN, Kuhns S, Neuner A, Hub B, Zentgraf H & Pereira G (2012) Cep164 mediates vesicular docking to the mother centriole during early steps of ciliogenesis. *J Cell Biol* 199: 1083–1101

Sedjaï F, Acquaviva C, Chevrier V, Chauvin J-P, Coppin E, Aouane A, Coulier F, Tolun A, Pierres M, Birnbaum D, *et al* (2010) Control of ciliogenesis by FOR20, a novel centrosome and pericentriolar satellite protein. *J Cell Sci* 123: 2391–2401

Shakya S & Westlake CJ (2021) Recent advances in understanding assembly of the primary cilium membrane. *Fac Rev* 10: 16

Shen Y, Wang H, Liu Z, Luo M, Ma S, Lu C, Cao Z, Yu Y, Cai R, Chen C, *et al* (2020) Identification of two novel pathogenic variants of PIBF1 by whole exome sequencing in a 2-year-old boy with Joubert syndrome. *BMC Med Genet* 21: 192

Sillibourne JE, Hurbain I, Grand-Perret T, Goud B, Tran P & Bornens M (2013) Primary ciliogenesis requires the distal appendage component Cep123. *Biol Open* 2: 535–545

Singla V, Romaguera-Ros M, Garcia-Verdugo JM & Reiter JF (2010) Ofd1, a human disease gene, regulates the length and distal structure of centrioles. *Dev Cell* 18: 410–424

Skouri F & Cohen J (1997) Genetic approach to regulated exocytosis using functional complementation in Paramecium: identification of the ND7 gene required for membrane fusion. *Mol Biol Cell* 8: 1063–1071

Sonneborn TM (1970) Gene action in development. *Proc R Soc Lond B Biol Sci* 176: 347–366

Sorokin S (1962) Centrioles and the formation of rudimentary cilia by fibroblasts and smooth muscle cells. *J Cell Biol* 15: 363–377

Steib E, Laporte MH, Gambarotto D, Olieric N, Zheng C, Borgers S, Olieric V, Le Guennec M, Koll F, Tassin A-M, *et al* (2020a) WDR90 is a centriolar microtubule wall protein important for centriole architecture integrity. *eLife* 9: e57205

Steib E, Laporte MH, Gambarotto D, Olieric N, Zheng C, Borgers S, Olieric V, Le Guennec M, Koll F, Tassin A-M, *et al* (2020b) WDR90 is a centriolar microtubule wall protein important for centriole architecture integrity. *eLife* 9: e57205

Stinchcombe JC, Randzavola LO, Angus KL, Mantell JM, Verkade P & Griffiths GM (2015) Mother Centriole Distal Appendages Mediate Centrosome Docking at the Immunological Synapse and Reveal Mechanistic Parallels with Ciliogenesis. *Curr Biol CB* 25: 3239–3244

Stowe TR, Wilkinson CJ, Iqbal A & Stearns T (2012) The centriolar satellite proteins Cep72 and Cep290 interact and are required for recruitment of BBS proteins to the cilium. *Mol Biol Cell* 23: 3322–3335

Tanos BE, Yang H-J, Soni R, Wang W-J, Macaluso FP, Asara JM & Tsou M-FB (2013) Centriole distal appendages promote membrane docking, leading to cilia initiation. *Genes Dev* 27: 163–168

Tassin AM & Bornens M (1999) Centrosome structure and microtubule nucleation in animal cells. *Biol Cell* 91: 343–354

Tassin A-M, Lemullois M & Aubusson-Fleury A (2015a) Paramecium tetraurelia basal body structure. *Cilia* 5: 6

Tassin A-M, Lemullois M & Aubusson-Fleury A (2015b) Paramecium tetraurelia basal body structure. *Cilia* 5: 6

Thauvin-Robinet C, Lee JS, Lopez E, Herranz-Pérez V, Shida T, Franco B, Jego L, Ye F, Pasquier L, Loget P, *et al* (2014) The oral-facial-digital syndrome gene C2CD3 encodes a positive regulator of centriole elongation. *Nat Genet* 46: 905–911

Thauvin-Robinet C, Thomas S, Sinico M, Aral B, Burglen L, Gigot N, Dollfus H, Rossignol S, Raynaud M, Philippe C, *et al* (2013) OFD1 mutations in males: phenotypic spectrum and ciliary basal body docking impairment. *Clin Genet* 84: 86–90

Vieillard J, Paschaki M, Duteyrat J-L, Augière C, Cortier E, Lapart J-A, Thomas J & Durand B (2016) Transition zone assembly and its contribution to axoneme formation in Drosophila male germ cells. *J Cell Biol* 214: 875–889

Vincensini L, Blisnick T & Bastin P (2011) 1001 model organisms to study cilia and flagella. *Biol Cell* 103: 109–130

Viol L, Hata S, Pastor-Peidro A, Neuner A, Murke F, Wuchter P, Ho AD, Giebel B & Pereira G (2020) Nek2 kinase displaces distal appendages from the mother centriole prior to mitosis. *J Cell Biol* 219

Wang L, Failler M, Fu W & Dynlacht BD (2018) A distal centriolar protein network controls organelle maturation and asymmetry. *Nat Commun* 9: 3938

Wang W-J, Tay HG, Soni R, Perumal GS, Goll MG, Macaluso FP, Asara JM, Amack JD & Tsou M-FB (2013) CEP162 is an axoneme-recognition protein promoting ciliary transition zone assembly at the cilia base. *Nat Cell Biol* 15: 591–601

Westlake CJ, Baye LM, Nachury MV, Wright KJ, Ervin KE, Phu L, Chalouni C, Beck JS, Kirkpatrick DS, Slusarski DC, *et al* (2011) Primary cilia membrane assembly is initiated by Rab11 and transport protein particle II (TRAPPII) complex-dependent trafficking of Rabin8 to the centrosome. *Proc Natl Acad Sci U S A* 108: 2759–2764

Wheway G, Schmidts M, Mans DA, Szymanska K, Nguyen T-MT, Racher H, Phelps IG, Toedt G, Kennedy J, Wunderlich KA, *et al* (2015) An siRNA-based functional genomics screen for the identification of regulators of ciliogenesis and ciliopathy genes. *Nat Cell Biol* 17: 1074–1087

Wiegering A, Dildrop R, Kalfhues L, Spychala A, Kuschel S, Lier JM, Zobel T, Dahmen S, Leu T, Struchtrup A, *et al* (2018) Cell type-specific regulation of ciliary transition zone assembly in vertebrates. *EMBO J* 37

Yang TT, Chong WM, Wang W-J, Mazo G, Tanos B, Chen Z, Tran TMN, Chen Y-D, Weng RR, Huang C-E, *et al* (2018) Super-resolution architecture of mammalian centriole distal appendages reveals distinct blade and matrix functional components. *Nat Commun* 9: 2023

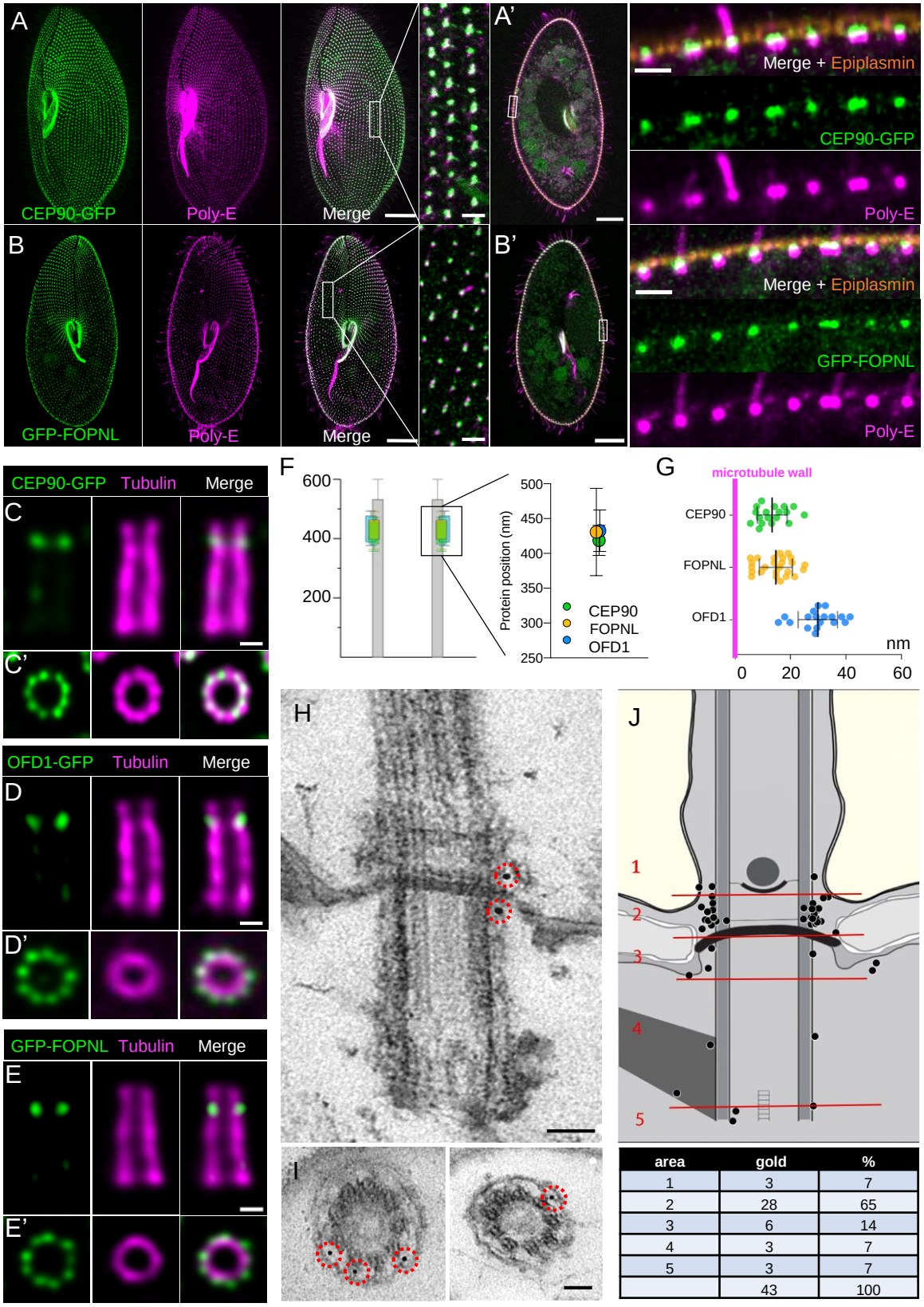

area	gold	%
1	3	7
2	28	65
3	6	14
4	3	7
5	3	7
	43	100

Figure 1

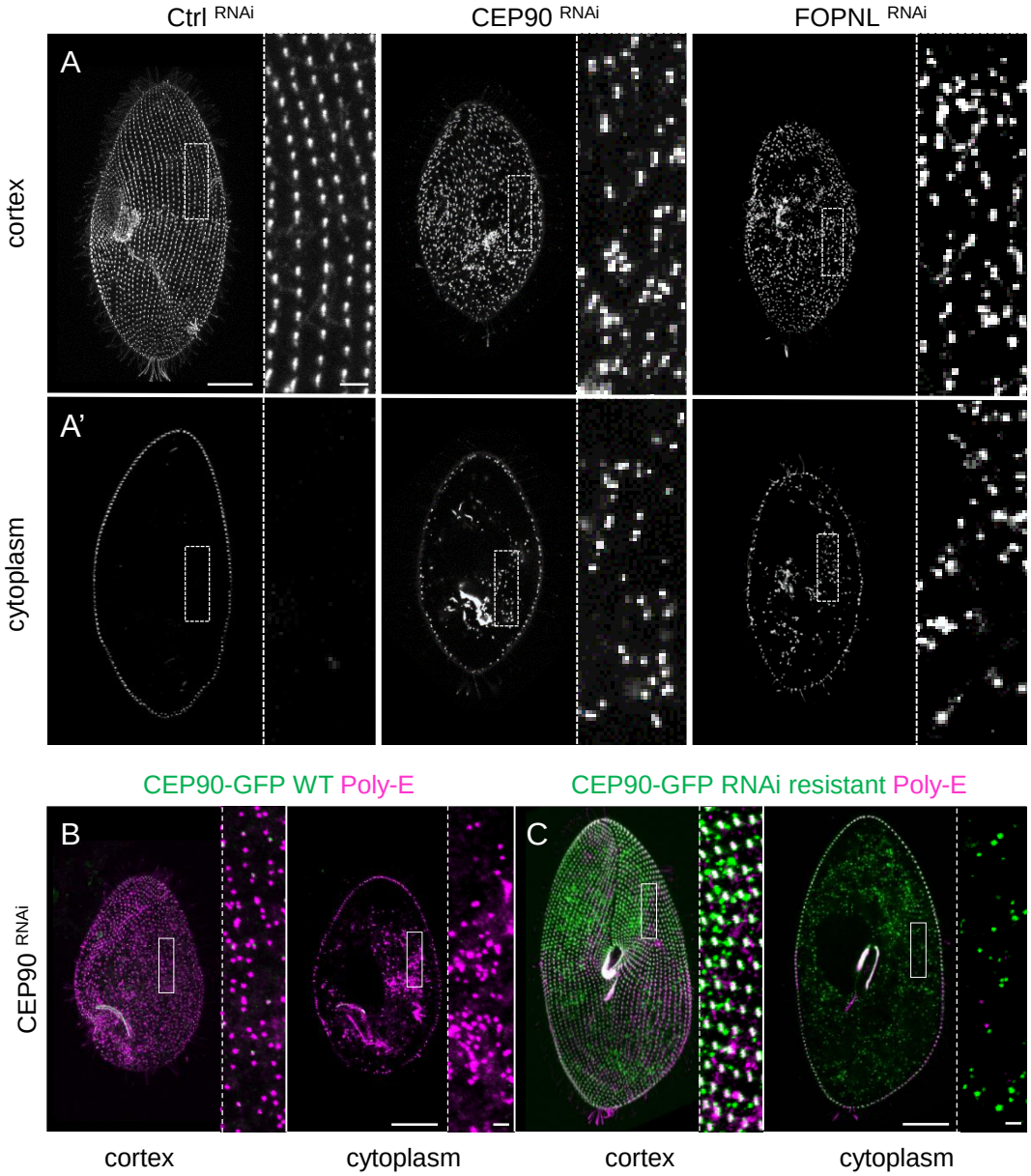
Ctrl RNAi
CEP90 RNAi
FOPNL RNAi
A
A'
cortex
cytoplasm
CEP90-GFP WT Poly-E
CEP90-GFP RNAi resistant Poly-E
B
C
CEP90 RNAi
cortex
cytoplasm
cortex
cytoplasm

Figure 2

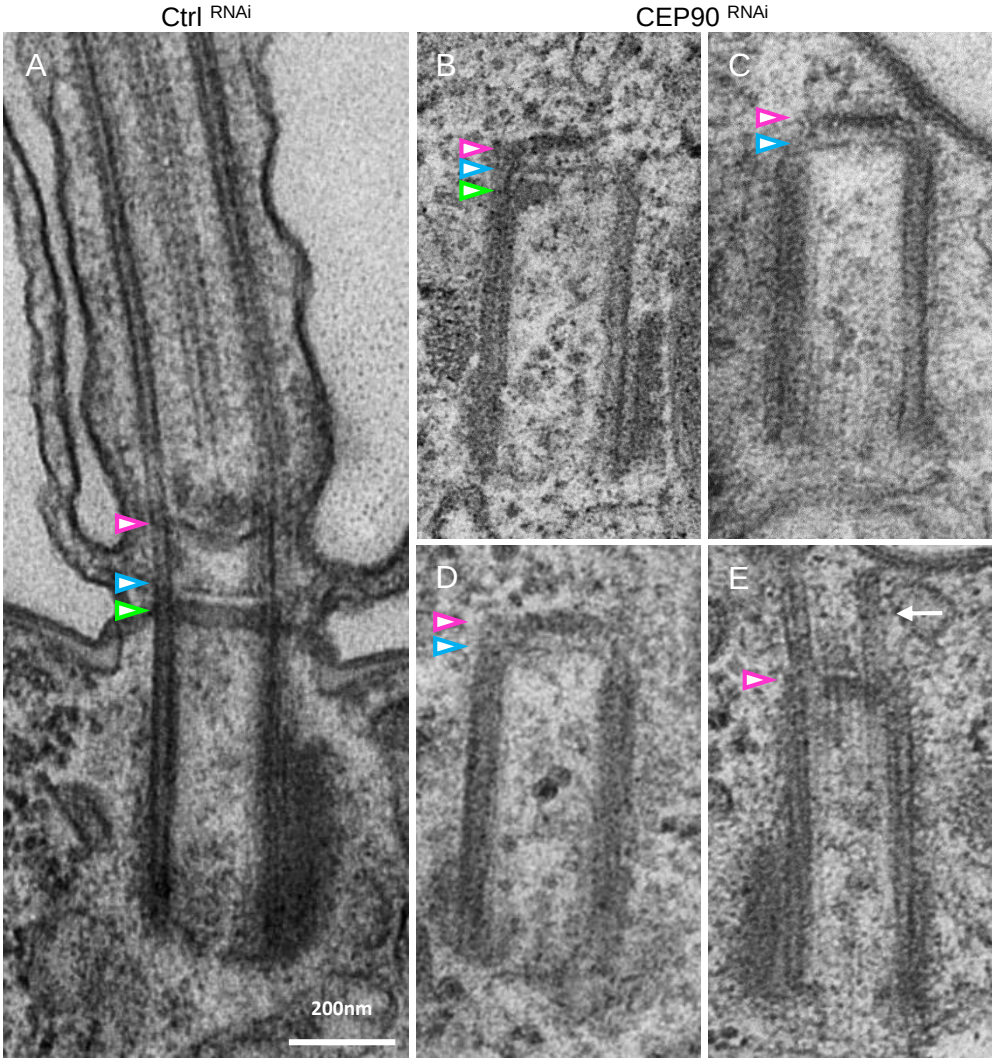

Figure 3

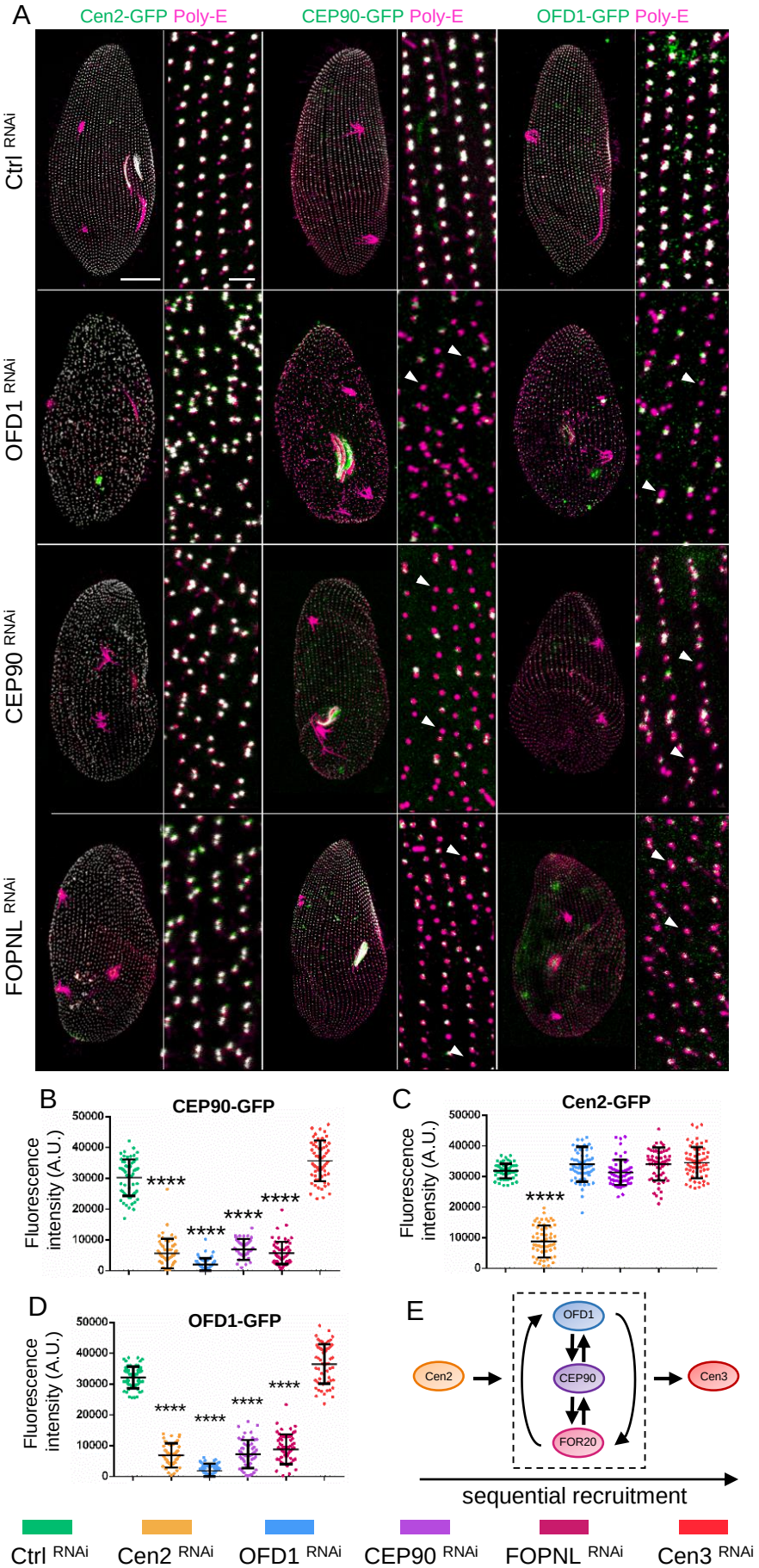
A
Cen2-GFP Poly-E
CEP90-GFP Poly-E
OFD1-GFP Poly-E
Ctrl RNAi
OFD1 RNAi
CEP90 RNAi
FOPNL RNAi
B
CEP90-GFP
Fluorescence intensity (A.U.)
50000
40000
30000
20000
10000
0
****
C
Cen2-GFP
D
OFD1-GFP
E
Cen2
OFD1
CEP90
FOR20
Cen3
sequential recruitment
Ctrl RNAi
Cen2 RNAi
OFD1 RNAi
CEP90 RNAi
FOPNL RNAi
Cen3 RNAi

Figure 4

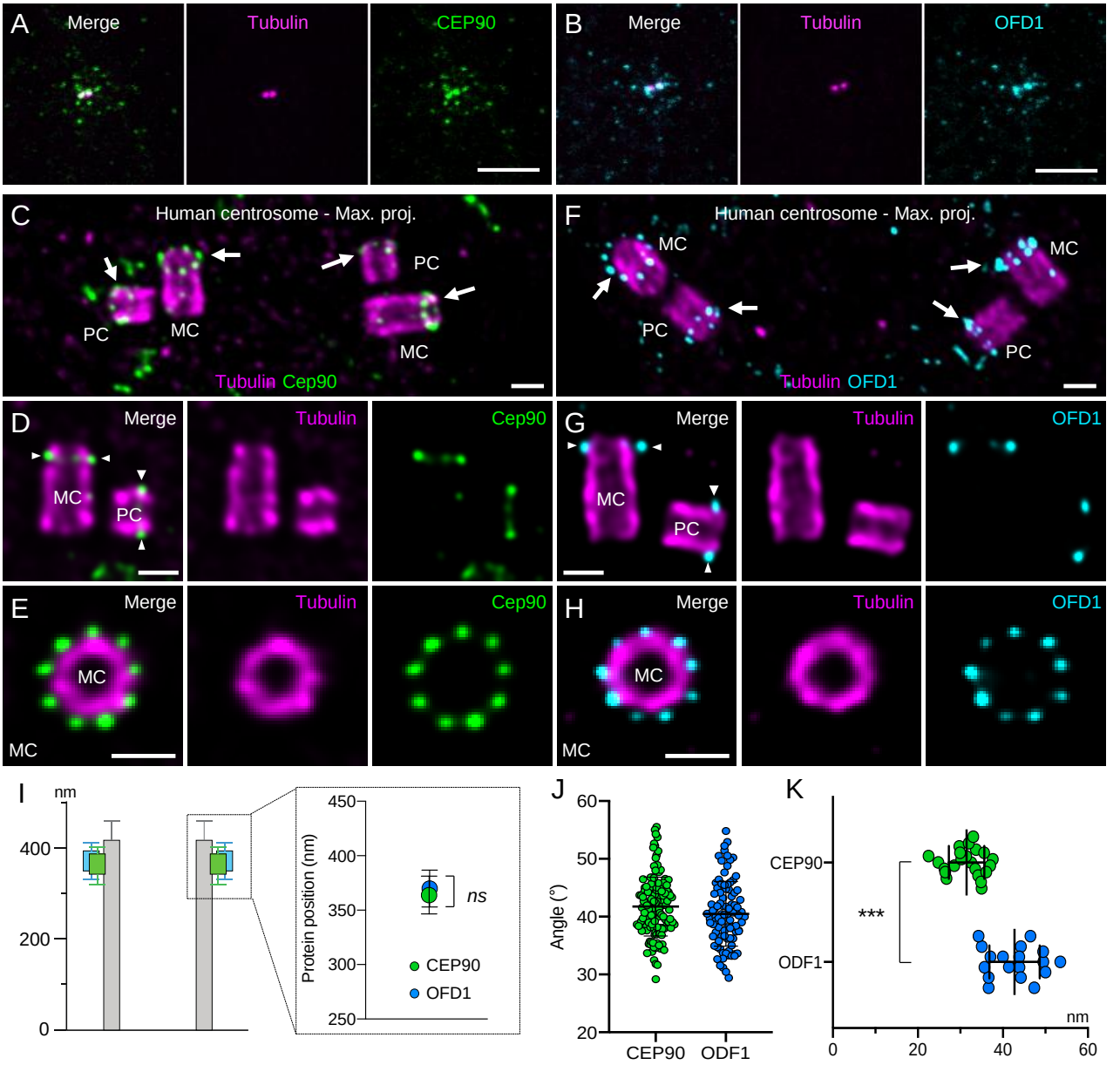
A
Merge
Tubulin
CEP90
B
Merge
Tubulin
OFD1
C
Human centrosome - Max. proj.
PC
MC
PC
MC
Tubulin Cep90
F
Human centrosome - Max. proj.
MC
MC
PC
PC
Tubulin OFD1
D
Merge
Tubulin
Cep90
MC
PC
G
Merge
Tubulin
OFD1
MC
PC
E
Merge
Tubulin
Cep90
MC
MC
H
Merge
Tubulin
OFD1
MC
MC
I
nm
400
200
0
450
400
350
300
250
Protein position (nm)
ns
CEP90
OFD1
J
60
50
40
30
20
Angle (°)
CEP90
ODF1
K
CEP90
ODF1
***
nm
0
20
40
60

Figure 5

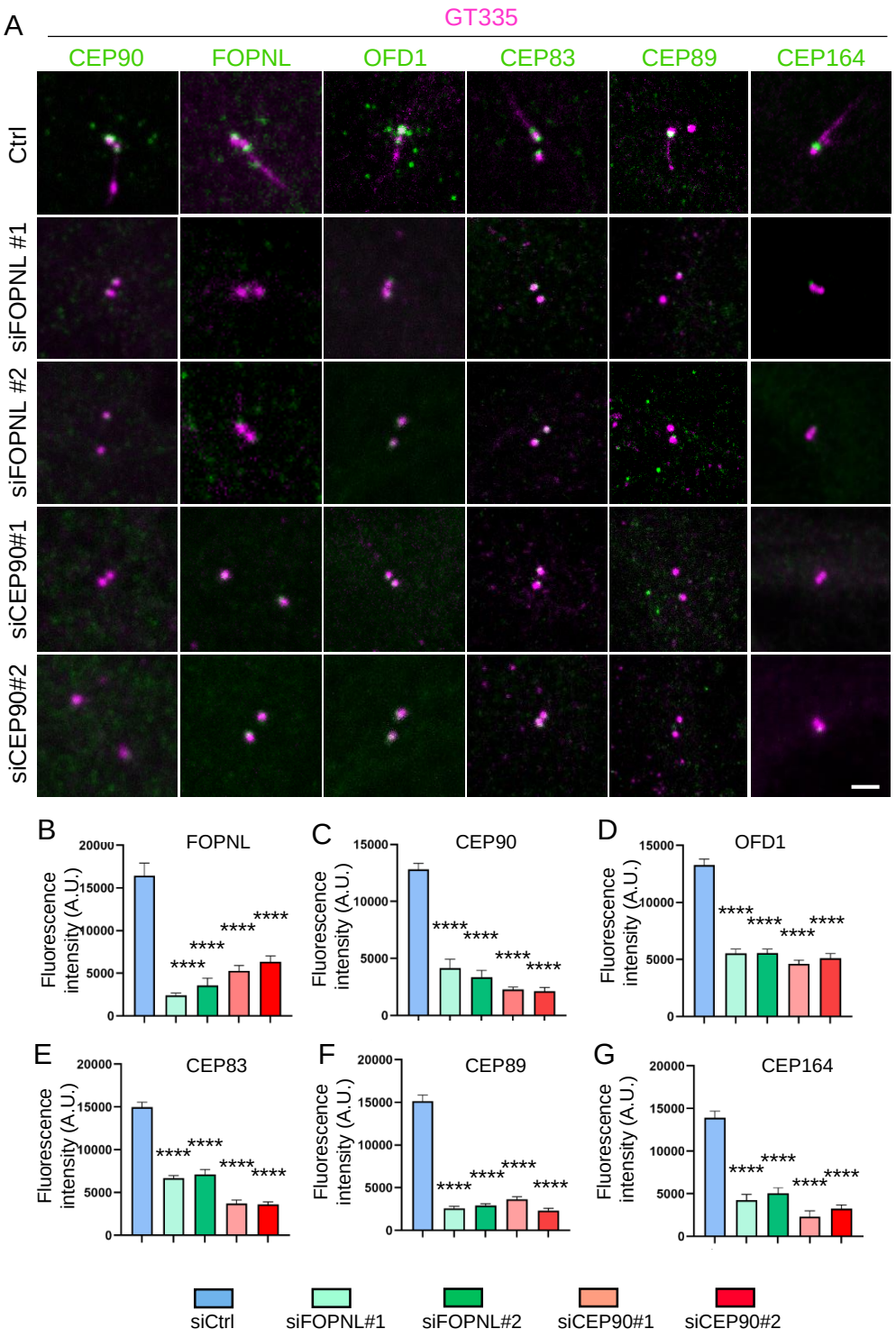
A
GT335
CEP90
FOPNL
OFD1
CEP83
CEP89
CEP164
Ctrl
siFOPNL #1
siFOPNL #2
siCEP90#1
siCEP90#2
B
FOPNL
C
CEP90
D
OFD1
E
CEP83
F
CEP89
G
CEP164
Fluorescence intensity (A.U.)
siCtrl
siFOPNL#1
siFOPNL#2
siCEP90#1
siCEP90#2

Figure 6

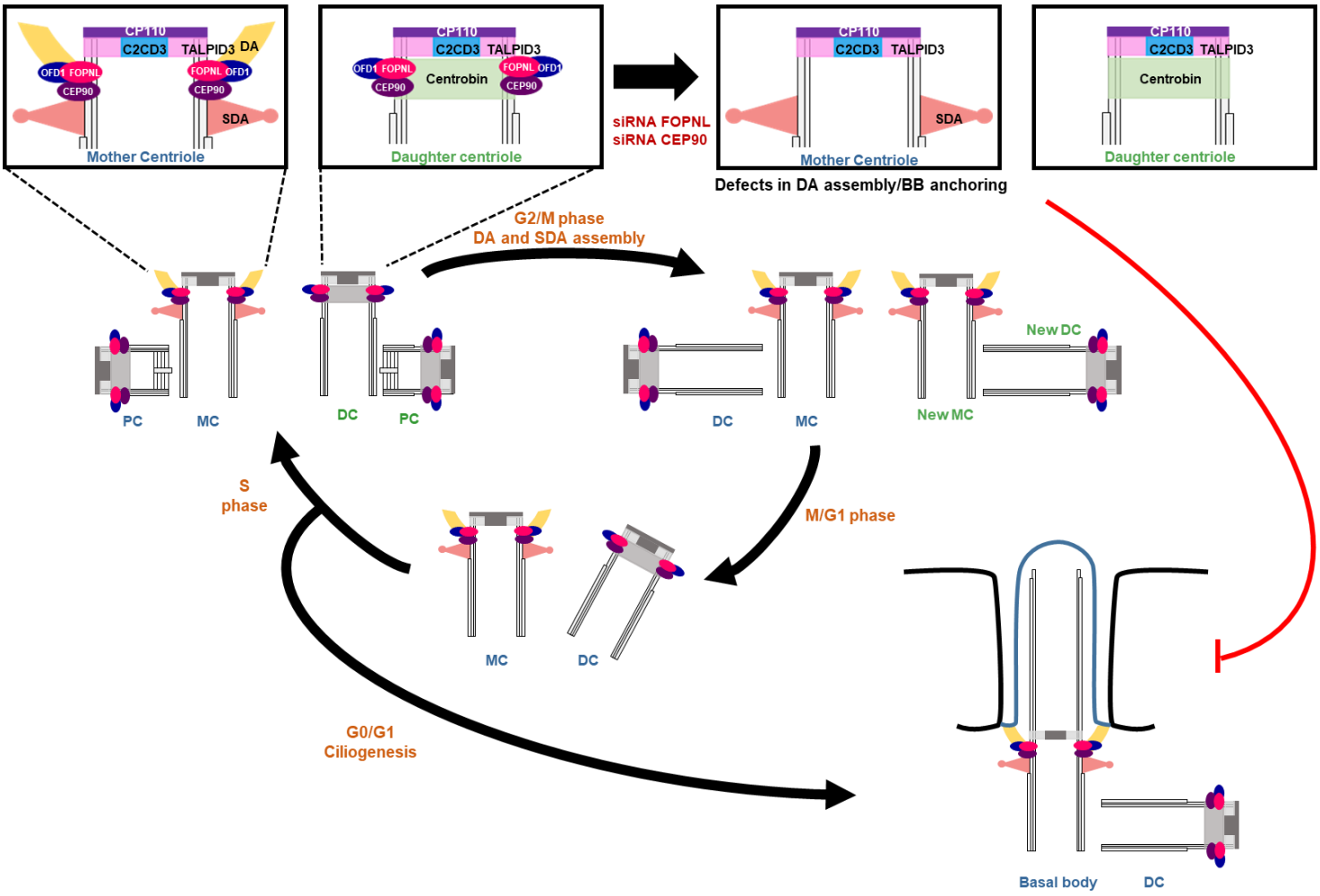
CP110
C2CD3
TALPID3
DA
OFD1
FOPNL
CEP90
SDA
Mother Centriole
Centrobin
Daughter centriole
siRNA FOPNL
siRNA CEP90
Defects in DA assembly/BB anchoring
G2/M phase
DA and SDA assembly
PC
MC
DC
New DC
New MC
S
phase
M/G1 phase
G0/G1
Ciliogenesis
Basal body

Figure 7